

Operational Metric for Quantum Chaos and the Corresponding Spatiotemporal-Entanglement Structure

Neil Dowling^{1,*} and Kavan Modi^{1,2,†}

¹*School of Physics & Astronomy, Monash University, Clayton, Victoria 3800, Australia*

²*Quantum for New South Wales, Sydney, New South Wales 2000, Australia*

 (Received 16 January 2023; revised 12 December 2023; accepted 19 December 2023; published 1 February 2024)

Chaotic systems are highly sensitive to a small perturbation and are ubiquitous throughout the biological sciences, the physical sciences, and even the social sciences. Taking this as the underlying principle, we construct an operational notion for quantum chaos. Namely, we demand that the future state of a many-body isolated quantum system is sensitive to past multitime operations on a small subpart of that system. By “sensitive,” we mean that the resultant states from two different perturbations cannot easily be transformed into each other. That is, the pertinent quantity is the complexity of the effect of the perturbation within the final state. From this intuitive metric, which we call the butterfly-flutter fidelity, we use the language of multitime quantum processes to identify a series of operational conditions on chaos; in particular, the scaling of the spatiotemporal entanglement. Our criteria already contain the routine notions, as well as the well-known diagnostics for quantum chaos. This includes the Peres-Loschmidt echo, dynamical entropy, tripartite mutual information, and local-operator entanglement. We hence present a unified framework for these existing diagnostics within a single structure. We also go on to quantify how several mechanisms, such as evolution generated from random circuits, lead to quantum chaos. Our work paves the way to systematically study many-body dynamical phenomena such as many-body localization, measurement-induced phase transitions, and Floquet dynamics.

DOI: [10.1103/PRXQuantum.5.010314](https://doi.org/10.1103/PRXQuantum.5.010314)

I. INTRODUCTION

Chaos as a principle is rather direct; a butterfly flutters its wings, which leads to an effect much bigger than itself. In other words, when something small leads to a very big effect. This effect arises in a vast array of fields, from economics and ecology to meteorology and astronomy, spanning disciplines and spatiotemporal scales.

Chaos at the microscale, on the other hand, is an exception. Quantum chaos is not well understood and lacks a universally accepted classification. There is a vast web of, often inconsistent, quantum chaos diagnostics in the literature [1], which leads to a muddy picture of what this concept actually means. In contrast, classically, chaos is a relatively complete framework. If one perturbs the initial conditions of a chaotic dynamical system, they see an

exponential deviation of trajectories in phase space, quantified by a Lyapunov exponent. Trying to naively extend this to quantum Hilbert space immediately falls short of a meaningful notion of chaos, as the unitarity of isolated quantum dynamics leads to a preservation of fidelity with time. How then, can there possibly be nonlinear effects resulting from the linearity of Schrödinger’s equation? We will see that the structure of entanglement holds the key to this conundrum.

Yet, much effort has been made to understand quantum chaos primarily as the cause of classical chaos [2–5], to identify the properties that an underlying quantum system requires in order to exhibit chaos in its semiclassical limit. An example of this is the empirical connection between random matrix theory and the Hamiltonians of classically chaotic systems [2]. Recently, with experimental access to complex many-body quantum systems with no meaningful classical limit, and given progress in related problems such as the black-hole information paradox [6,7] and the quantum foundations of statistical mechanics [8–10], quantum chaos as a research program has seen renewed interest across a range of research communities. In this context, a complete structure of quantum chaos, independent of any classical limit, is highly desirable but remains absent.

*neil.dowling@monash.edu

†kavan.modi@monash.edu

Published by the American Physical Society under the terms of the [Creative Commons Attribution 4.0 International](https://creativecommons.org/licenses/by/4.0/) license. Further distribution of this work must maintain attribution to the author(s) and the published article’s title, journal citation, and DOI.

In this work, we approach quantum chaos from an operational, and theory agnostic, principle: *chaos is a deterministic phenomenon, where the future state has a strong sensitivity to a local perturbation in the past*. For quantum processes, the key ingredient will turn out to be spatiotemporal entanglement. To get there, we first identify the underlying definition of chaos as a starting point and build a quantum butterfly-flutter process from this fundamental principle. With this, we construct a genuinely quantum measure for chaos, based solely on this statement, which we term the *butterfly-flutter fidelity*. This relies on the intuition that it is the complexity induced by a perturbation in the resultant future pure state, rather than just orthogonality, that dictates a chaotic effect. We adapt this principle into the theory of quantum processes and exploit their multitime structures. Namely, we use a tool from quantum information theory—process-state duality—to determine a hierarchy of necessary conditions on meaningful notions of chaos in many-body systems. These conditions culminate into the novel strong metric of the butterfly-flutter fidelity.

Figure 1 breaks up the problem of quantum chaos into three broad components, laying out a review of the landscape of this multidisciplinary field and contextualizing our results. Figure 1(a) represents the mechanisms by which quantum chaos arises. Our contribution, depicted in Fig. 1(b), is to identify a strong, operational criterion for quantum chaos through sensitivity in a future state, to the spatiotemporal quantum entanglement of the corresponding process. We propose that this intuitive metric bridges the gap between the mechanisms in Fig. 1(a) and the signatures for chaos depicted in Fig. 1(c). We provide explicit connections between several elements of these panels in this work, the details of which we outline below.

Specifically, affirming the validity of our approach, we show that our criterion is stronger than and encompasses existing dynamical signatures of chaos. We show this explicitly for the Peres-Loschmidt echo, dynamical entropy, tripartite mutual information, and local-operator entanglement [20]. That is, we identify the underlying structure leading to characteristic chaotic behavior of each

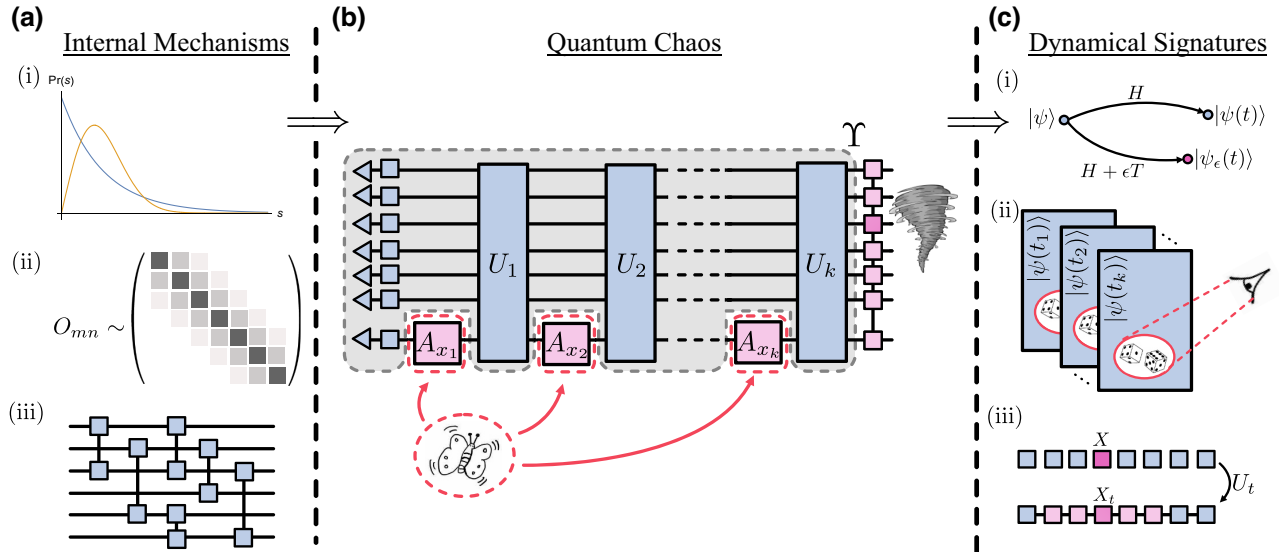


FIG. 1. A schematic of the causes, structure, and effects of quantum chaos. (a) The internal mechanisms of chaos are the intrinsic properties of the dynamics that lead to chaotic effects: e.g., properties of the Hamiltonian such as (i) level-spacing statistics and (ii) the eigenstate thermalization hypothesis (ETH), or properties of the quantum circuit describing the dynamics such as (iii) whether it forms a unitary design. (b) In this work, we will identify general quantum butterfly flutter protocol and from this argue that chaos reduces to a hierarchy of conditions on the process describing the dynamics, including the volume-law spatiotemporal-entanglement structure. This principle forms the stepping stone between causal mechanisms of chaos and observable diagnostics of chaos. We remark that we only conjecture that level-spacing statistics and ETH [see (a)(i) and (a)(ii)] lead to quantum chaos as formalized in this paper and that these relationships form an interesting open question. (c) Operational diagnostics for quantum chaos. Some popular probes include (i) The Peres-Loschmidt echo, also known as fidelity decay or the Loschmidt echo, which is the measure of the deviation between states, for evolution under a perturbed compared to an unperturbed Hamiltonian [11, 12]; (ii) The dynamical entropy, which quantifies how much information one gains asymptotically from repeatedly measuring a subpart of a quantum system [3, 13–15]; and (iii) local-operator entanglement, which measures the complexity of the state representation of a time-evolved Heisenberg operator [16–18]. Another example that we analyze in this work (not shown) is the tripartite mutual information, which measures the entanglement properties of a state representation of a local input space of a channel together with a bipartition of the output space [19].

of these popular chaos diagnostics. We offer a clear hierarchy of conditions of a chaotic effect, due to a “butterfly flutter,” unifying a range of (apparently) inconsistent diagnostics.

Next, we show that there are several known mechanisms for quantum processes that lead to quantum chaos. In particular, we show that both Haar-random unitary dynamics and random circuit dynamics—which lead to approximate t -design states—are highly likely to generate processes that satisfy our operational criterion for quantum chaos. Our results also open up the possibility of systematically studying other internal mechanisms thought to generate quantum chaos, e.g., Wigner-Dyson statistics [2] or the eigenstate thermalization hypothesis (ETH) [21–23].

Finally, our approach is different from previous works that have usually relied on averages over Haar and/or thermal ensembles to draw connections between some previous signatures for quantum chaos [24–26]. We work solely within a deterministic pure-state setting, identifying a series of conditions that stem from a sensitivity to past local operations, without any need to average over operators or dynamics. Moreover, other metrics for quantum chaos also start from the notion of a kind of a butterfly effect, such as the out-of-time-order correlator (OTOC) [27]. However, our sense of this intuitive idea is different and does not necessarily suffer the same shortfalls as, e.g., the OTOC, which decays quickly even for some integrable systems [28–30].

A. Summary of main result

We first give an informal explanation of the main innovation of this work. We use a simplified formalism and setup in order to convey the main ideas, with a more detailed exposition to be given later.

Consider an isolated quantum system where a sequence of k unitaries A_{x_i} are applied on a local subspace S , such that the global system is defined on the Hilbert space $\mathcal{H}_S \otimes \mathcal{H}_E$. Later, we will call this sequence a *butterfly flutter* and allow it to consist of an arbitrary sequence of rank-1 instruments (Definition 1). The outgoing state after this protocol is

$$|\Upsilon_{R|\vec{x}}\rangle = A_{x_k} U_k \cdots A_{x_2} U_2 A_{x_1} U_1 |\psi_{SE}\rangle, \quad (1)$$

where U_i represents global unitary evolution, either Floquet or according to a Hamiltonian for time t_i , and where $A_{x_i} \equiv (A_{x_i})_S \otimes \mathbb{1}_E$. The other choices of notation will become apparent in the following sections.

Now, we similarly introduce a strictly different set of k unitaries, labeled by the list \vec{y} . We take these unitaries to be orthogonal to the first choice, in the Hilbert-Schmidt sense such that $\text{tr}[A_{x_i}^\dagger A_{y_j}] = 0$ for all $i \in [1, k]$. Note that we impose no such constraint on operations for different times, A_{x_i} compared to A_{x_j} with $i \neq j$. We later loosen this condition such that these can be, collectively, approximately

orthogonal operations. The outgoing state is defined analogously to Eq. (1), with the same global dynamics U_i and subsystem decomposition $\mathcal{H}_S \otimes \mathcal{H}_E$ but different unitary “perturbations.” We can then ask: how much do these two resultant states, $|\Upsilon_{R|\vec{x}}\rangle$ and $|\Upsilon_{R|\vec{y}}\rangle$, differ?

This question is a direct translation to quantum mechanics of the principle of chaos as a sensitivity perturbation. The task is to define exactly what we mean by this sensitivity. As already discussed, fidelity is preserved under unitary evolution. Further, as we discuss in Sec. III A and Appendix E, the fidelity cannot be the full story: most dynamics, irrespective of integrability, will lead to a small fidelity $|\langle \Upsilon_{R|\vec{x}} | \Upsilon_{R|\vec{y}} \rangle|^2$. We will show that this orthogonality translates into an entropic condition on the underlying process for this perturbation protocol, namely, that a genuinely chaotic system should necessarily have a volumetrically scaling spatiotemporal entanglement.

We instead strengthen this by defining a new metric to compare these states, which we call the *butterfly-flutter fidelity* (Definition 2). This compares how different the two final states are in a complexity sense, and measures the fidelity after what we call a correction unitary V :

$$\zeta := \sup_{V \in \mathcal{R}} (|\langle \Upsilon_{R|\vec{x}} | V | \Upsilon_{R|\vec{y}} \rangle|^2). \quad (2)$$

This quantity is depicted graphically in Fig. 4(a). Here, \mathcal{R} is a restricted set of unitaries on $\mathcal{H}_S \otimes \mathcal{H}_E$, which for now can be considered to be the set of simple (low-depth) circuits. Intuitively, this measure in Eq. (2) determines whether or not the orthogonality between $\Upsilon_{R|\vec{x}}$ and $\Upsilon_{R|\vec{y}}$ is complex. That is, is the sensitivity stemming from past perturbations (local unitaries) easily correctable? Based on our operational criteria for quantum chaos, we argue that the dynamics are chaotic if this not easily correctable—when $\zeta \approx 0$ for an appropriately defined set of corrections \mathcal{R} and for any choice of butterfly flutters. This notion of chaos then allows us to identify a connection with entanglement properties of the underlying process describing the “butterfly flutter” protocol.

For example, one could choose two butterfly flutters as a sequence of k Pauli X gates on a single qubit of a many-body system at k times and the other to be a series of identity maps (do nothing). With free global evolution occurring between each gate, the butterfly-flutter fidelity in Eq. (2) would then indicate that the dynamics is chaotic if the fidelity between the final states is small, $\zeta \approx 0$, even after trying to align the two final states using any small-depth local circuit V . This quantity is the main focus of this work.

The rest of the paper is structured as follows. In Sec. II, we review the tools that we require to characterize quantum chaos and the butterfly-flutter fidelity. This predominantly includes the theory of multitime quantum process [31–33], which allows us to describe all possible perturbations and resultant effects within a single quantum state.

Then, in Sec. III, we present a set of increasingly strong necessary conditions on a dynamical process for which $\zeta \approx 0$ in Eq. (2). These conditions are all motivated from the principle of chaos as a sensitivity to perturbation and start with a minimal sense of what a large effect could be, stemming from a past local perturbation. This main-results section then culminates in the butterfly-flutter fidelity, as the strongest condition in this hierarchy. We conclude this section by comparing the butterfly-flutter fidelity to the classical ideas of chaos and detailing how one could, in principle, measure it in experiment.

In Sec. IV, we support the proposed conditions by showing how a range of previous dynamical signatures of chaos agree with them, as depicted in Fig. 1. We summarize these connections in Fig. 2, which serves as a summary of this work and the related work of Ref. [30]. Finally, in Sec. V, we discuss mechanisms of chaos that lead to the operational effects that we propose. In particular, we prove that random dynamics—both fully Haar random and those generated by unitary designs—typically lead to chaos.

II. TOOLS: MULTITIME QUANTUM PROCESSES AND SPATIOTEMPORAL ENTANGLEMENT

Many of the results of this work rely on the application of ideas from entanglement theory to multitime quantum processes, in order to interpret the overarching problem of chaos in isolated many-body systems. We here give only an overview of the relevant facets of this topic and refer the reader to Appendix A for more information and to Refs. [33,34] for a more complete introduction to the process-tensor framework.

Consider a finite-dimensional quantum system. A quantum process is a quantum dynamical system under the effect of multitime interventions on some accessible local space \mathcal{H}_S . These interventions are described by instruments, which are trace nonincreasing quantum maps. The dynamics between interventions can then be dilated to a system and environment $\mathcal{H}_S \otimes \mathcal{H}_E$, such that the total isolated state on $\mathcal{H}_S \otimes \mathcal{H}_E$ evolves unitarily on this extended space. A k -step process tensor is the mathematical description of a such a process, encoding all possible spatiotemporal correlations in a single object—analogue to how a density matrix encodes single-time measurements.

In this work, we will generally consider rank-1 instruments, such as unitary matrices and projective measurements (including the outgoing state). In this case, we are able to write down the full pure state on $\mathcal{H}_S \otimes \mathcal{H}_E$ at the end of this process,

$$|\psi'_{SE}\rangle = U_k A_{x_k} U_{k-1} \dots U_1 A_{x_1} |\psi_{SE}\rangle, \quad (3)$$

where we have rewritten this as the conditional state of a subpart of process $|\Upsilon\rangle$, and we will explain exactly

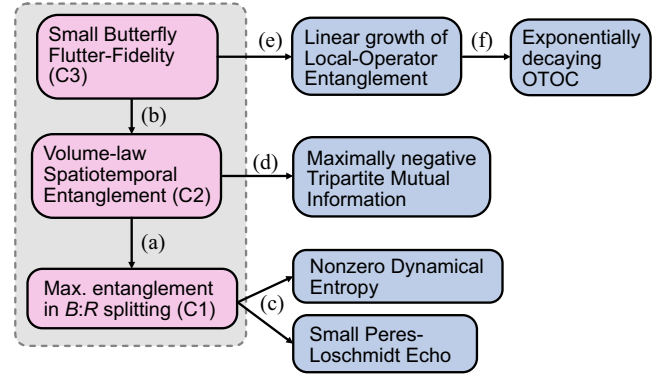


FIG. 2. A summary of the results of this work, where directed arrows mean implication. The shaded region with pink boxes is the hierarchy of conditions on quantum chaos as a sensitivity to perturbation proposed in this work, (C1)–(C3). (a) The volume-law spatiotemporal entanglement of $|\Upsilon\rangle$ is strictly stronger than maximum entanglement in the single bipartition $B : R$. (b) A small butterfly-flutter fidelity (Definition 2) necessarily implies the volume-law spatiotemporal entanglement of $|\Upsilon\rangle$ (Proposition 2), with equivalence when the initial state is area-law (Proposition 3). (c) The (Trotterized) Peres-Loschmidt echo constitutes the particular case of an asymptotically many-time weak unitary butterfly flutter (Sec. IV A), while an extensive dynamical entropy is equivalent to an extensive entanglement scaling in the splitting $B : R$ (Proposition 1 and Sec. IV B). (d) For a single-time butterfly flutter, volume-law spatiotemporal entanglement directly implies a (near) maximally negative tripartite mutual information of the corresponding channel (Proposition 6). (e) For a single-time butterfly flutter, if the butterfly-flutter fidelity is small for any initial state, then for an operator entanglement complexity measure, the local-operator entanglement grows linearly with time (Theorem 2). (f) If the local-operator entanglement grows linearly with time, then general OTOCs necessarily decay exponentially [30].

what this means below. A_{x_i} can be arbitrary norm non-increasing operators, with $\sum_{x_i} A_{x_i}^\dagger A_{x_i} = \mathbb{1}$; i.e., anything that maps pure states to (possibly subnormalized) pure states. This includes, e.g., unitary operators or projective measurements. We stress that A_{x_i} are considered to act locally on \mathcal{H}_S , such that $A_{x_i} \equiv A_{x_i}^{(S)} \otimes \mathbb{1}^{(E)}$. As everything is pure here, there is no need to consider superoperators or density matrices and left multiplication by matrices is a sufficient description (for the mixed-state extension of this, see Appendix A). $|\Upsilon_{R|\bar{x}}\rangle$ could be a subnormalized pure state if, e.g., the instruments are chosen to be a series of projective measurements,

$$|\psi'_{SE}\rangle = \sqrt{p_{\bar{x}}} |\Upsilon_{R|\bar{x}}\rangle. \quad (4)$$

Here, $A_{x_i} = |x_i\rangle\langle x_i|$, $p_{\bar{x}}$ is the probability of observing this outcome, and we have neglected the (unobservable) global phase. We will usually consider the (normalized) conditional state $|\Upsilon_{R|\bar{x}}\rangle$ when investigating chaotic effects, as we

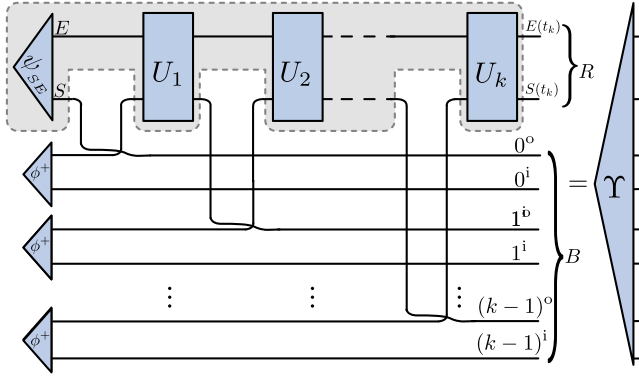


FIG. 3. The tensor-network diagram of the protocol producing the Choi state of a pure process tensor through the generalized Choi-Jamiołkowski isomorphism [31,36]. This means that input indices are put on equal footing with output indices, through appending a maximally entangled ancilla system $|\phi^+\rangle$ at each time and inserting half of this state into the process. The final output state of this protocol encodes all multitime spatiotemporal correlations: a pure process tensor. A multitime expectation value can then be computed in this representation by finding the Hilbert-Schmidt inner product between this (normalized) Choi state and the (supernormalized) Choi state of a multitime instrument. The system \mathcal{H}_S denotes the single-time space where instruments act and the environment \mathcal{H}_E the dilated space such that all dynamics are unitary. Here, the independent Hilbert spaces are labeled such that $(\ell)^{\ddagger}$ ($(\ell)^{\circ}$) is the input (output) system space \mathcal{H}_S at time t_ℓ , showing that the final output $|\Upsilon\rangle$ corresponds to a $(2k+2)$ -body pure quantum state.

will be concerned with the resultant state rather than the probability that it is produced.

Rather than choosing a particular instrument A_{x_i} for each intervention, one can instead feed in half of a maximally entangled state from an ancilla space, as shown in Fig. 3. This results in the pure state $|\Upsilon\rangle$, encoding both any interventions on the multitime space in the past, which we call \mathcal{H}_B , and the final pure state on the global isolated system, on the space \mathcal{H}_R . This is the generalized Choi-Jamiołkowski isomorphism (CJI) [31,32], shown in Fig. 3. Alternatively to this ancilla-based construction, the pure process tensor can be defined succinctly as

$$|\Upsilon\rangle := |U_k\rangle * \cdots * |U_1\rangle * |\psi_{SE}(t_1)\rangle, \quad (5)$$

where $*$ is the *link product*, corresponding to composition of maps within the Choi representation [35], and is essentially a matrix product on the \mathcal{H}_E space and a tensor product on the \mathcal{H}_S space. A ket of a rank-1 instrument A corresponds to the single-time Choi state

$$|A\rangle := (A \otimes \mathbb{1}) |\phi^+\rangle, \quad (6)$$

by the usual single-time CJI: channel-state duality [34].

Here, we have gathered the multitime Hilbert space where the full multitime instruments act on a space with

the single label,

$$\mathcal{H}_B \equiv \mathcal{H}_{S(t_{k-1})}^{\text{io}} \cdots \otimes \mathcal{H}_{S(t_1)}^{\text{io}} \otimes \mathcal{H}_{S(t_0)}^{\text{io}}, \quad (7)$$

called the “butterfly” space \mathcal{H}_B , where $\mathcal{H}_{S(t_j)}^{\text{io}} \equiv \mathcal{H}_{S(t_j)}^{\text{i}} \otimes \mathcal{H}_{S(t_j)}^{\text{o}}$. \mathcal{H}^{i} represents the input space to the process, while \mathcal{H}^{o} represents the output. The “remainder” space \mathcal{H}_R —the full final state on the system plus environment at the end of the protocol, where the “butterfly” does not act—is

$$\mathcal{H}_R \equiv \mathcal{H}_{S(t_k)}^{\text{o}} \otimes \mathcal{H}_{E(t_k)}^{\text{o}}. \quad (8)$$

All of these are clearly labeled in Fig. 3. It will become apparent in Sec. III why we name these spaces as such.

From Eq. (5), we can determine the outgoing (possibly subnormalized) state in Eq. (4) from projections on this state,

$$|\psi'_{SE}\rangle = \langle \vec{x} | \Upsilon \rangle. \quad (9)$$

For independent instruments at each intervention time, we have that

$$|\vec{x}\rangle := |x_k\rangle \otimes \cdots \otimes |x_1\rangle, \quad (10)$$

where each single-time state is constructed as in Eq. (6). Alternatively, one could trace over the final state on \mathcal{H}_R and the reduced state on \mathcal{H}_B , Υ_B , is the process tensor [31–33], as we describe in Appendix A.

The key point here is that through the CJI we have reduced all possible correlations of a dynamical multitime experiment to a single quantum state, $|\Upsilon\rangle$. This means that all the machinery from many-body physics is available to describe multitime effects. A subtle difference from the single-time case is that the normalization of these Choi states do not exactly correspond to the normalization of states and projections. Instruments are taken to be supernormalized, while processes have unit normalization and so constitute valid quantum states

$$\langle \Upsilon | \Upsilon \rangle = 1, \quad \text{and} \quad \langle \vec{x} | \vec{x} \rangle \leq d_S^{2k}, \quad (11)$$

where the inequality is saturated for deterministic instruments: completely positive trace-preserving completely-positive trace-preserving (CPTP) maps. This normalization ensures that one gets well-defined probabilities in Eq. (4).

Therefore, dynamical properties of a process such as non-Markovianity [32,33,37–39], temporal correlation function equilibration [40,41], whether its measurement statistics can be described by a classical stochastic process [42–44], multipartite entanglement in time [45], and other many-time properties [46] can all be clearly defined

in terms of properties of the quantum state $|\Upsilon\rangle$. However, the spatiotemporal-entanglement structure of this multi-time object is largely unexplored and we will show that this has vast implications for understanding quantum chaotic versus regular dynamics.

Any pure quantum state $|\psi\rangle_{AB}$ on $\mathcal{H}_A \otimes \mathcal{H}_B$ can be decomposed across any bipartition $A : B$ via the Schmidt decomposition,

$$|\psi\rangle_{AB} = \sum_{i=1}^{\chi} \lambda_i |\alpha_i\rangle_A |\beta_i\rangle_B, \quad (12)$$

where $\langle \alpha_i | \alpha_j \rangle = \delta_{ij} = \langle \beta_i | \beta_j \rangle$. χ is called the *bond dimension* or *Schmidt rank*, which dictates intuitively the extent to which the subsystems are entangled with each other. The bond dimension is equal to one if and only if the state is separable across $A : B$.

Using the decomposition given in Eq. (12), one can successively increase the size of the subsystem \mathcal{H}_A and determine how the bond dimension scales. We will deal with one-spatial-dimension systems when discussing spatiotemporal entanglement in this work, as characteristic entanglement scaling depends on the underlying geometry [47]. Our results should generalize in a straightforward way to higher spatial dimensions. If χ is bounded by $\min\{d_A, D\}$ for a constant $D < (d_A d_B)/2$ for any \mathcal{H}_A with dimension d_A up to half the total Hilbert-space dimension,

this is called area-law scaling. In this case, for example, a one-dimensional spin-chain state may be written efficiently as a matrix product state (MPS) [47–50]. Despite being introduced in order to efficiently simulate the ground state of certain Hamiltonians, it was soon realized that a fundamental property of a state written as an MPS is revealed in the scaling of the bond dimension [51]. On the other hand, if the bond dimension scales (approximately) extensively with the subsystem size, this is volume-law scaling. This directly implies a characteristically scaling entanglement entropy,

$$S(\rho_A) \propto \log(d_A), \quad (13)$$

where $S(\rho_A)$ is the von Neumann entropy of the reduced state ρ_A . Area-law can be defined formally as a bounded entanglement with scaling subsystem size, for all Rényi entropies [49]. Such scaling will synonymously be called *entanglement structure* or *entanglement scaling* throughout this work. We will show that this property within the pure process tensor $|\Upsilon\rangle$ is intrinsically linked to the chaoticity of a quantum process.

We will now delve into our main result, interpreting the dynamical meaning behind the spatiotemporal-entanglement structure of quantum processes.

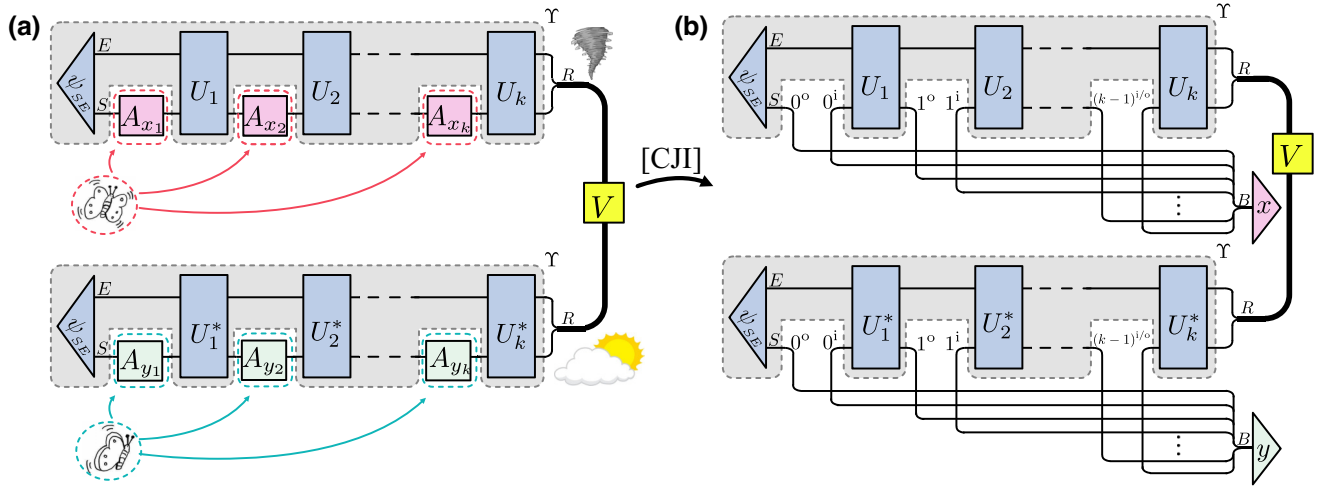


FIG. 4. Two equivalent representations of the butterfly-flutter fidelity (see Definition 2). (a) The process representation of the butterfly-flutter fidelity. Two orthogonal sequences of instruments, $\{A_{x_i}\}$ and $\{A_{y_i}\}$, act k times on the system Hilbert space denoted by \mathcal{H}_S , of a time-evolving state $|\psi_{SE}\rangle$. The final pure states on $\mathcal{H}_R = \mathcal{H}_S \otimes \mathcal{H}_E$ can be compared, with a simple correction unitary V (partially) aligning the states, which enforces that the effect of the butterfly flutter is complex on the final states. This is Eq. (22) in the text. (b) Using the CJI, as described in Sec. II and Fig. 3, the process corresponding to the butterfly protocol can be mapped one to one to a quantum state $|\Upsilon\rangle \in \mathcal{H}_B \otimes \mathcal{H}_R$. Then, the butterfly-flutter fidelity given in Eq. (22) corresponds to projecting onto the butterfly space \mathcal{H}_B with two orthogonal projections, $\langle \vec{x} |$ and $\langle \vec{y} |$, and comparing the resulting conditional states on \mathcal{H}_R . This allows us to interpret strong and complex effects due to the butterfly flutter in terms of the entanglement properties of $|\Upsilon\rangle$: a strong effect from entanglement in the bipartition $B : R$ (Proposition 1) and a complex effect from volume-law entanglement in the full state (Proposition 3).

III. MAIN RESULT: THE BUTTERFLY-FLUTTER FIDELITY AND SPATIOTEMPORAL-ENTANGLEMENT

In Sec. II, we have defined a pure process tensor $|\Upsilon\rangle$ that encodes an experiment where a local part \mathcal{H}_S of a many-body quantum system is interacted with across k times, together with the outgoing pure state on the space \mathcal{H}_R . The multitime intervention, which we call a butterfly flutter and is defined explicitly in Definition 1, is taken to act on the collective multitime “butterfly” space \mathcal{H}_B [see Eq. (7)]. This formalism will allow us to identify necessary conditions stemming from the principle of quantum chaos as a sensitivity to perturbation, in terms of the properties of the state $|\Upsilon\rangle$. Figure 4 offers a graphical representation of the state-process duality that serves as a key tool of our analysis.

We will now identify a series of conditions on the process $|\Upsilon\rangle$, each stronger than the previous, such that if a process satisfies (C3), then it also necessarily satisfies (C2) and hence also (C1). We make an intuitive argument based on chaos as a sensitivity to perturbation, to argue for each condition. We will show in Sec. IV that they are each related to previous signatures of chaos (see also Fig. 1).

(C1) (*Perturbation orthogonalizes future state.*) The final state on R should be strongly sensitive to butterfly flutters on B .

(C2) (*Scrambling as volume-law entanglement.*) Butterfly flutters on B should affect a large portion of the final state on R .

(C3) (*Complexity of sensitivity.*) Different butterfly flutters on B should lead to different enough states on R , in a complexity sense.

From each of these, we will identify the properties of $|\Upsilon\rangle$ to which these conditions lead. Of course, as written above, these conditions are informal statements. We will spend the rest of this section making this precise and restate this list at the end in full technical detail.

A. Sensitivity to perturbation (C1)

Given a sequence of small interventions on a many-body system, what is the minimal effect on the final pure state such that it is sufficiently perturbed? As a minimal condition, we argue that a perturbation should orthogonalize this final state, in the usual sense of fidelity. We will show that this leads to a simple entropic condition on the pure process state $|\Upsilon\rangle$.

More technically, we first define explicitly what we mean by a perturbation that probes chaos.

Definition 1.—A butterfly flutter is a multitime linear map with some outcome label \vec{x} , defined by k rank-1 instruments $\{A_{x_1}, A_{x_2}, \dots, A_{x_k}\}$, which maps a k -time pure

process $|\Upsilon\rangle \in \mathcal{H}_B \otimes \mathcal{H}_R$ to a normalized state,

$$\frac{\langle \vec{x} | \Upsilon \rangle}{\sqrt{\langle \Upsilon | \vec{x} \rangle \langle \vec{x} | \Upsilon \rangle}} = |\Upsilon_{R|\vec{x}}\rangle. \quad (14)$$

Here, $|\vec{x}\rangle \in \mathcal{H}_B$ is the Choi state of the multitime instrument that defines the butterfly flutter, as in Eq. (10), and the (conditional) output state $|\Upsilon_{R|\vec{x}}\rangle$ is defined in Eq. (16).

Note that butterfly flutters are distinct from the multitime instruments discussed in Sec. II only in that we take the normalized output from its action. This is important, as we do not wish to consider the probability of a butterfly to occur, only its effect. $|\Upsilon_{R|\vec{x}}\rangle$ is just the conditional pure state on the global $\mathcal{H}_S \otimes \mathcal{H}_E$ space.

We can compare the two final conditional (pure) states after two distinct butterfly flutter protocols labeled by \vec{x} and \vec{y} :

$$\mathcal{D}(|\Upsilon_{R|\vec{x}}\rangle, |\Upsilon_{R|\vec{y}}\rangle). \quad (15)$$

Here, \mathcal{D} is some metric on pure quantum states, naturally taken to be the fidelity, and the label $\vec{w} = (w_1, \dots, w_k) \in \{\vec{x}, \vec{y}\}$ denotes instruments acting at k times, such that

$$|\Upsilon_{R|\vec{w}}\rangle := \frac{A_{w_k} U_k \cdots A_{w_2} U_2 A_{w_1} U_1 |\psi_{SE}\rangle}{\sqrt{\langle \psi_{SE} | U_1^\dagger \cdots A_{w_k}^\dagger A_{w_k} \cdots U_1 | \psi_{SE} \rangle}}. \quad (16)$$

This is a bipartite quantum state after a butterfly flutter protocol, which may include a sequence of measurements and preparations on some local system labeled \mathcal{H}_S , recording the outcomes as \vec{w} . Alternatively, A_{w_i} could be a unitary on some subspace or any other quantum operation, which could even be correlated across multiple times. Note that if two butterflies only consist of unitary maps, then the normalization in the denominator of Eq. (16) is simply equal to one. In the interest of identifying the general form of any quantum butterfly effect, we allow the perturbation to be any pure multitime instrument.

Condition (C1) then means that

$$|\langle \Upsilon_{R|\vec{x}} | \Upsilon_{R|\vec{y}} \rangle|^2 \approx 0, \quad (17)$$

for any two orthogonal butterfly flutters $|\vec{x}\rangle$ and $|\vec{y}\rangle$. Our construction of dynamical quantum chaos then reduces to a static property of a process: given two nondeterministic projections on some small subsystem, how do the left-over states compare? (C1) states that for a chaotic process, butterflies need to have a large effect as in Eq. (17).

We now ask what property of the many-time state $|\Upsilon\rangle$ leads to the behavior Eq. (17)? We summarize in Fig. 4 the butterfly-flutter fidelity given in Eq. (22) in the equivalent Choi and operator representations. We have done the conceptual heavy lifting in the setup of this problem and so the following result is rather direct.

Proposition 1.—For any two orthogonal butterflies, one obtains (approximately) orthogonal final states on \mathcal{H}_R if and only if $|\Upsilon\rangle$ is (approximately) maximally entangled across the bipartition $B : R$.

Proof for this and all further results in this section can be found in Appendix B.

We note that the previous signature of dynamical entropy turns out to be exactly the scaling of the entanglement of $|\Upsilon\rangle$ in $B : R$ with times k and the fidelity $|\langle \Upsilon_{R|\bar{x}} | \Upsilon_{R|\bar{y}} \rangle|^2$ is a Trotterized generalization of the Peres-Loschmidt echo. We show this in Sec. IV with a detailed exposition on the relation between our conditions (C1)–(C3) and previous signatures (see also Fig. 1). Proposition 1 then gives a novel connection between these two previously well-studied metrics of chaos.

B. Scrambling as spatiotemporal entanglement (C2)

The condition in Sec. III A cannot be a complete notion of quantum chaos. In fact, most systems will look “chaotic” according to the prescription (C1). For example, circuit dynamics consisting solely of SWAP gates, without any interactions, leads exactly to Eq. (17) being satisfied. In this case, the “orthogonality” of the butterflies is transferred to some large environment and a new pure state is accessed on the butterfly space with each step. The orthogonalization resulting from a butterfly flutter resides entirely in a small subspace of \mathcal{H}_R , yet could be misconstrued as a strong global effect. We look at this example in more detail in Appendix E and name such dynamics as a *Lindblad-Bernoulli shift* [52]. As a further example, it can be shown analytically that free fermions lead to a (maximal) linearly growing dynamical entropy of a process [53], which by Proposition 1 means that Eq. (17) is also true.

We therefore now introduce a notion of scrambling to the entropic measure from Sec. III A. Instead of just specifying that the entanglement in the splitting $B : R$ of the purified process $|\Upsilon\rangle$ is volume-law with increasing k , we extend this to incorporate that the effect of the butterfly flutter spreads nonlocally. We do this by including a subpart of the butterfly space together with a subpart of the final pure state when looking at an entanglement bipartition of the process. In particular, (C2) means that

$$S(\Upsilon_{B_1 R_1}) \propto \log(d_{B_1} d_{R_1}), \quad (18)$$

where S here indicates von Neumann entropy, R_1 and R_2 are a bipartition of the final state, $\mathcal{H}_R =: \mathcal{H}_{R_1} \otimes \mathcal{H}_{R_2}$, and, similarly, $\mathcal{H}_B =: \mathcal{H}_{B_1} \otimes \mathcal{H}_{B_2}$. We will generally consider bipartitions $R_1 : R_2$ such that $d_{B R_1} < d_{R_2}$. Equation (18) means that the entanglement of $|\Upsilon\rangle$ in the arbitrary splitting $B_1 R_1 : B_2 R_2$ needs to be volume-law. Often, we choose $S(\Upsilon_{B R_1})$ to investigate the spatial scrambling of the interventions from the entire space \mathcal{H}_B . In this case, spatiotemporal entanglement of the process $|\Upsilon\rangle$ serves as a

multitime generalization of “strong scrambling” in terms of the tripartite mutual information [19] (see Sec. IV C).

There are two subtle considerations to take into account here. For one, explicitly defining a “volume-law” compared to an “area-law” entanglement scaling requires specifying the underlying geometry. For the $B : R$ entanglement of (C1), there is a natural one-dimensional scaling through increasing the number of times k on which \mathcal{H}_B is defined (and suitably redefining $|\Upsilon\rangle$ in each case). When discussing spatiotemporal entanglement, we require a (varying) bipartition of the spatial part of the process on \mathcal{H}_R , as well as the temporal part \mathcal{H}_B . For (C2), we therefore restrict ourselves to systems of one spatial dimension but note that one could likely generalize these results to higher dimensions. In addition, if the dynamics are chosen to be local, as is often the physically relevant situation, the space \mathcal{H}_{R_1} should be chosen to be causally connected to the space B , i.e., well within the Lieb Robinson “light cone” of the past space \mathcal{H}_B [54,55]. This ensures that the operations on \mathcal{H}_B may be possibly correlated with \mathcal{H}_{R_1} . This is immediately clear in circuit models of dynamics, where the light cone is exact with a sharp cutoff [56,57]. Beyond this, it would be interesting to investigate this further with precise Lieb-Robinson bounds, along the lines of Ref. [58].

Equation (18) then means that rather than the butterfly flutter only affecting some localized part of the final pure state on R (as in the Lindblad-Bernoulli shift; see Appendix E), leading to a high entanglement in the splitting $B : R$, Eq. (18) means that its effect spreads globally. This is what we call volume-law spatiotemporal entanglement. We will further argue that this is the essence of quantum chaos: that large effects from small past operations correspond exactly to an extensive entropy scaling with increasing size of R_1 , for a given B (and possible bipartition B_1).

An example tensor network for computing this quantity is given in Fig. 5, for a one-dimensional lattice system. Here, λ_i represents the Schmidt coefficient across the bipartition $B : R$, while the (yellow) circles represent bonds within a MPS representation of the final spatial pure state on R . A volume-law spatiotemporal entanglement then means a maximum bond dimension across any of these yellow circle bonds within R , when the B subsystem can be connected to any of the components of R within this tensor network (represented by grayed-out bonds).

But is this spatiotemporal entanglement detectable? If one measures the final-state fidelity as in Eq. (17), such that the butterfly flutters $|\bar{x}\rangle$ and $|\bar{y}\rangle$ include part of the final state, R_1 , we will see that these butterfly flutters typically distinguish between area-law and volume-law spatiotemporal entanglement in $|\Upsilon\rangle$. We will do this by choosing random and unitary butterfly flutters on $\mathcal{H}_B \otimes \mathcal{H}_{R_1}$ and determining the fidelity (22) for these.

In the following, $\mathbb{P}_{a \sim \mu}$ and $\mathbb{E}_{a \sim \mu}$ will mean, respectively, the probability and expectation value of the sampling of a random variable a over the measure μ . $\mu = \mathbb{H}$ denotes the

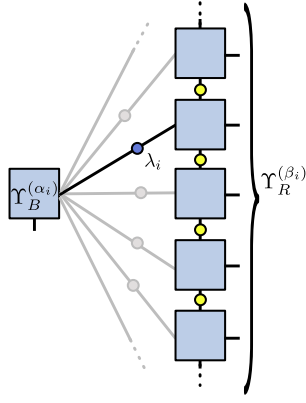


FIG. 5. A spatiotemporal tensor network of the process representing the butterfly protocol. Condition (C2) states that a chaotic process will have maximal Schmidt rank across a decomposition across any cut (represented by colored circles)—i.e., that this network has a maximal bond dimension. These cuts are restricted to be only within the light cone of the butterfly flutter in the final state on \mathcal{H}_R . The grayed-out lines represent other possible bonds in the choice of the space \mathcal{H}_{R_1} in Eq. (22), which should all pertain to a maximal bond dimension (volume-law) tensor network. The tensors (blue squares) on the right-hand side have a local dimension of d_{R_1} and additionally should have maximal bond dimension between them for a chaotic process.

Haar measure—the unique unitarily invariant measure on Hilbert space. More details on randomness in Hilbert space are given in Sec. V.

Theorem 1.—(Random Butterflies Are Likely to Detect Spatiotemporal Entanglement) For a Haar-random choice of orthogonal butterflies $\mathcal{X} = \{|\vec{x}\rangle, |\vec{y}\rangle\}$ across the combined space $\mathcal{H}_B \otimes \mathcal{H}_{R_1}$ for any choice of space \mathcal{H}_{R_1} , the fidelity of the final state is likely to be sensitive to the volume-law property of $|\Upsilon\rangle$. In particular, for $\delta > 0$,

$$\mathbb{P}_{\mathcal{X} \sim \mathbb{H}} \left\{ |\langle \Upsilon_{R_2|\vec{x}} | \Upsilon_{R_2|\vec{y}} \rangle|^2 \geq \delta \right\} \lesssim \frac{\text{tr}[\Upsilon_{BR_1}^2] - 1/(d_{BR_1})}{\delta}, \quad (19)$$

where $d_{BR_1} = d_B d_{R_1}$. This inequality is slightly approximated for large $d_{BR_1}^2$, such that $d_{BR_1}^2 \pm 1 \approx d_{BR_1}^2$.

A proof for this can be found in Appendix B. This result is also valid for sampling a random butterfly from a 2-design rather than fully Haar random, which can be done efficiently in practice.

This constitutes a concrete connection between the fidelity between final states in Eq. (17) and spatiotemporal entanglement of the pure process $|\Upsilon\rangle$. The key point is that for volume-law entanglement of the process $|\Upsilon\rangle$, the purity of the reduced state on $\mathcal{H}_B \otimes \mathcal{H}_{R_1}$ is inversely proportional to the size of the subsystem,

$$\text{tr}[\Upsilon_{BR_1}^2] \sim \mathcal{O}\left(\frac{1}{d_{BR_1}}\right). \quad (20)$$

For a Choi state that is truly volume-law—rather than just maximally entangled across some specific splitting—this is the case for *any* choice of \mathcal{H}_{R_1} up to causality considerations. So for volume-law, the right-hand side of Eq. (B5) is close to zero for almost any small $\delta > 0$. Therefore, for most random unitary butterflies, ζ in Eq. (22) will likely be small for volume-law processes.

Note that framing chaos in terms of the entanglement properties of $|\Upsilon\rangle$ is independent of the instrument, i.e., the butterfly flutter represented by $|\vec{x}\rangle$. This allows for testing of this principle against any previous or new heuristic of quantum chaos. It also implies that the manifestation of quantum chaos may be tested for strong or weak butterflies, and many-time or few-time, which turns out to be a key distinction between the Peres-Loschmidt echo and local-operator entanglement, as we show in Sec. IV.

One might now want to know if volume-law spatiotemporally entangled processes exist; if the condition (C2) is too strong. In fact, from concentration-of-measure results, it is known that most processes generated from Haar-random dynamics are locally exponentially close to the completely noisy process [59],

$$\text{tr}_R[|\Upsilon^{(\mathbb{H})}\rangle \langle \Upsilon^{(\mathbb{H})}|] \approx \frac{\mathbb{1}}{d_B}, \text{ for } d_B \ll d_R \quad (21)$$

and polynomially close for dynamics sampled from an ϵ -approximate t -design [60]. Such a process also has volume-law spatiotemporal entanglement, as we prove in Sec. V.

We now move to our final condition on quantum chaos.

C. Complexity of sensitivity to perturbation (C3)

We now introduce a final, strictly stronger, measure of chaos, based on a notion of the complexity distance between final states, after two distinct butterfly flutters. This is not just a fidelity measure like the ones we have considered so far but, rather, the fidelity after a restricted correction.

Definition 2.—The butterfly-flutter fidelity takes values between $0 \leq \zeta \leq 1$ and is defined as

$$\zeta(\Upsilon) := \sup_{V \in \mathcal{R}, \langle \vec{x} | \vec{y} \rangle = 0} (|\langle \Upsilon_{R|\vec{x}} | V | \Upsilon_{R|\vec{y}} \rangle|^2). \quad (22)$$

Here, V is a unitary operation on the full (spatial) Hilbert space \mathcal{H}_R and is restricted to some low-complexity set $\mathcal{R} \subset \mathbb{U}(d_R)$.

Note that often in Eq. (22) we will instead choose a particular pair of butterfly flutters $|\vec{x}\rangle$ and $|\vec{y}\rangle$ or otherwise average over some set of them. This is order to perform analytic calculations or to draw comparisons with other quantities and the interpretation of a sensitivity to perturbation holds true without an optimization over all possible butterfly flutters satisfying $\langle \vec{x} | \vec{y} \rangle = 0$.

Intuitively, the butterfly-flutter fidelity measures how difficult it is to convert one resultant state $\Upsilon_{R|\bar{x}}$ to the other $\Upsilon_{R|\bar{y}}$. In other words, it measures how easily correctable the effect of a past butterfly flutter is. We leave open the exact measure of the complexity with which the ‘‘correction’’ unitary V is restricted. Possible choices include specifying V to be: a constant-depth local circuit, independent of the system size or time evolution in the process; a local circuit with depth proportional to the size of the system d_R but independent of the time of evolution; a unitary with an appropriately defined restricted Nielsen complexity [61]; or an matrix product operator (MPO) of restricted (constant) bond dimension. Of course, many of these measures are related. It would be an interesting avenue of future research to investigate this quantity in more detail and for different models. For the rest of this work, we will generally take V such that it can be represented by an MPO with a restricted bond dimension, part of the set \mathcal{R}_{MPO} . Therefore, a process will be chaotic according to (C3) if it is not possible to efficiently correct the effects of a past butterfly flutter. We note that the butterfly-flutter fidelity reduces to simply the fidelity, as in (C1) and Eq. (17), when V is restricted to the identity $\mathcal{R} = \{1\}$.

We will now show that this is a strictly stronger condition than volume-law spatiotemporal entanglement; that (C3) \implies (C2).

Proposition 2.—If the butterfly-flutter fidelity given in Eq. (22) is not, $\zeta \approx 0$, then the process $|\Upsilon\rangle$ has volume-law spatiotemporal entanglement.

A proof for this can be found in Appendix B. The question remains of just how strong the condition (C3) is. That is, when is there volume-law spatiotemporal entanglement in a process (C2) but the effects of a butterfly flutter are easily correctable? In fact, the only case where (C2) and (C3) are not equivalent is if the process has a volume-law initial state.

Proposition 3.—If the butterfly-flutter fidelity given in Eq. (22) is not small (nonchaotic), $\zeta \approx 1$, but the process $|\Upsilon\rangle$ has volume-law spatiotemporal entanglement, the process can be written in terms of simple dynamics with a volume-law entangled initial state.

A proof for this can be found in Appendix B. What this result means is that in the particular case where a process is regular according to (C3) but chaotic according to (C2), then all the volume-law entanglement is attributed to the initial state. The dynamics part of the process can be considered to have area-law entanglement.

In the setup we have suggested to classify chaos in quantum systems, one interacts locally with a quantum system across multiple times and examines the effect on the final global pure state. In this situation, the above result (Proposition 3) means that in terms of the entanglement properties of the corresponding process $|\Upsilon\rangle$, one cannot distinguish between a process that first prepares a volume-law spatial entanglement state from a process

that genuinely creates volume-law spatiotemporal entanglement from the dynamics. One way to interpret this is that complex spatial entanglement in itself is chaotic. We refer to this as quantum *state chaos*: for a volume-law entangled state, performing an operation on a small part of a large state instantaneously has a highly nonlocal and strong effect on the remainder of the state.

This also follows from the fact that a multipartite quantum state is also a quantum channel, through teleportation. This is a purely quantum effect and thus there is no classical analogue to quantum state chaos. Volume-law spatiotemporal entanglement is equivalent to chaos in the sense of a strong nonlocal sensitivity to perturbations, regardless of whether these perturbations occur simultaneously to the effect (state chaos) or in the past with the effect stemming from dynamics [as measured by the butterfly-flutter fidelity (C3)]. However, in the traditional dynamical sense, the butterfly-flutter fidelity measures the chaoticity of the dynamics and so can be seen as equivalent to the quantum butterfly effect: the operationally meaningful notion of quantum chaos.

D. Sensitivity to initial perturbations

The above operational understanding for quantum chaos readily resolves a fundamental question. Namely, are quantum chaotic systems sensitive to an initial perturbation?

The usual argument against a quantum sensitivity to perturbation is that the distance (or fidelity) between two initial states, $\epsilon = |\langle\psi|\phi\rangle|$, is preserved with unitary time evolution

$$|\langle\psi|U_i^\dagger U_i|\phi\rangle| = |\langle\psi|\phi\rangle| = \epsilon. \quad (23)$$

This precludes a straightforward notion of exponential (or otherwise) deviation with respect to ϵ .

(C3) includes a rather direct and intuitive notion of sensitivity to initial conditions. Consider a single-time butterfly flutter protocol, with perturbative operations, X and Y , on initial state $|\psi\rangle$. Equation (22) then reduces to a sensitivity of the resultant state after this initial operation:

$$\zeta(\Upsilon) = \sup_{V \in \mathcal{R}} \left(|\langle\psi|X^\dagger U_i^\dagger V U_i Y|\psi\rangle|^2 \right). \quad (24)$$

Here, we have assumed that the local perturbations $X \equiv (X_S \otimes \mathbb{1}_E)$ are unitary for simplicity and so the final states are normalized. Instead of comparing the final-state fidelity given an initially perturbed state as in Eq. (23), the single-time flutter corresponds to how difficult it is to correct the resultant state from a local perturbation. This notion of difficulty encompasses the complexity inherent to quantum mechanics but admits the classical analogue of sensitivity to perturbation.

E. Determining the butterfly flutter protocol in the laboratory

The quantum butterfly protocol in Eq. (22) is a fidelity of final pure states, which apparently requires a backward-in-time global evolution to compute. In this section, we show that by appending a quantum ancilla space to the protocol, one can compute ζ through only forward-in-time evolution.

Consider the same setup as the butterfly flutter protocol in Eq. (22), with appended qubit ancilla space \mathcal{H}_A , with combined initial state

$$|\psi_{SEA}\rangle = |\psi\rangle_{SE} \otimes |+\rangle_A. \quad (25)$$

Here, the subscripts S , E , and A denote system, environment and ancilla Hilbert spaces respectively. Then, for a butterfly flutter defined by the unitary instruments $A_{x_1}, A_{x_2}, \dots, A_{x_k}$ acting on \mathcal{H}_S , define an instrument at time t_i on the full $\mathcal{H}_S \otimes \mathcal{H}_E \otimes \mathcal{H}_A$ space as

$$A'_i := \mathbb{1}_E \otimes (A_{x_i} \otimes |0\rangle\langle 0| + A_{y_i} \otimes |1\rangle\langle 1|). \quad (26)$$

We also define an additional (controlled) instrument which encodes the correction unitary V :

$$V' := \mathbb{1}_{SE} \otimes |0\rangle\langle 0| + V \otimes |1\rangle\langle 1|. \quad (27)$$

Then, the final state of the reduced state of the ancilla qubit at the end of the forward-in-time evolution of the butterfly protocol is

$$\rho = \text{tr}_{SE}[\mathcal{V}' \mathcal{U}_k A'_k \dots \mathcal{U}_1 A'_1 (|\psi_{SEA}\rangle \langle \psi_{SEA}|)], \quad (28)$$

where, as is standard throughout this work, calligraphic script letters correspond to superoperators, $\mathcal{A}'_i(\cdot) \equiv A'_i(\cdot) A_i^\dagger$, $\mathcal{V}'(\cdot) \equiv V'(\cdot) V'^\dagger$, and $\mathcal{U}'_i(\cdot) \equiv U'_i(\cdot) U_i^\dagger$ is global unitary $\mathcal{H}_S \otimes \mathcal{H}_E$ evolution. This protocol is presented in Fig. 6. Then it is easy to check that the squared off-diagonal elements of the final state of the ancilla qubit give exactly the butterfly-flutter fidelity of Eq. (22), for a given choice of correction unitary V . Further, the off-diagonal elements of a density matrix are easily measurable:

$$\zeta = |\langle 0|\rho|1\rangle|^2 = \left| \frac{1}{2} \langle \sigma_x + i\sigma_y \rangle \right|^2. \quad (29)$$

This can be directly generalized to larger ancilla spaces, if one wants to try a set of different butterfly flutters.

We will finish this section by making some remarks about the limitations of a realistic experimental setup. In a nonisolated situation where the initial state may be mixed and where evolution may not be unitary, then Eq. (28) takes

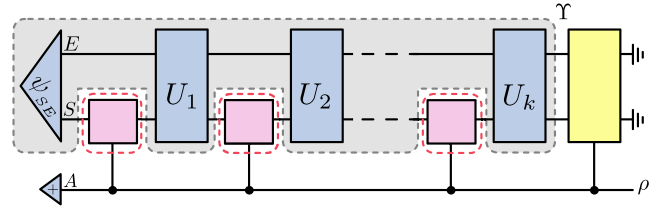


FIG. 6. The forward-in-time protocol for measuring the butterfly-flutter fidelity. Here, the pink controlled operations correspond to the butterfly flutters $|\bar{x}\rangle$ for an ancilla qubit equal to $|0\rangle\langle 0|$ and $|\bar{y}\rangle$ for an ancilla qubit equal to $|1\rangle\langle 1|$. The (yellow) global operation at the end (rightmost) is then similarly controlled to be either the identity map or the correction unitary V to be optimized over [see the discussion around Eq. (22)]. The butterfly-flutter fidelity is then stored in the coherences of the final state of the ancilla, ρ , while information of decoherence effects is encoded in the diagonals.

the form

$$\rho = \text{tr}_{SE}[\mathcal{V}' \mathcal{A}'_k \mathcal{L}_{k-1} \dots \mathcal{A}'_1 \mathcal{L}_1(\rho_i)]. \quad (30)$$

Here, ρ_i is some arbitrary initial state and \mathcal{L}_i represents open quantum system evolution, which may include arbitrary decoherence effects (\mathcal{L}_i is generally a CPTP map). In practice, Eqs. (28) and (30) require an identical protocol from a (hypothetical) experimenter. In practice, one cannot easily tell whether the scaling of the butterfly-flutter fidelity is according to Eq. (30) or the perfectly isolated Eq. (28). This is a problem faced with other measures of the quantum case (such as the OTOC) and, indeed, even classically it is difficult to discern between noise and dynamical chaos.

In the butterfly-flutter fidelity protocol, one can check the unitarity of the dynamics by checking the purity of the final total state. This requires access to two copies of the final state to perform a SWAP test. One alternative to this setup is to perform the butterfly flutter protocol with the correction unitary coming from the set of all possible unitaries, $\mathcal{R} = \mathbb{U}(d_R)$ in Eq. (22). This means that the correction unitary V will align the resultant states $\Upsilon_{R|\bar{x}}$ and $\Upsilon_{R|\bar{y}}$ to give $\zeta = 1$ if the dynamics are unitary [following Eq. (28)]. If the dynamics were not unitary [Eq. (30)], this would not be possible and so in this case we have $\zeta < 1$. Of course, it is highly expensive and nontrivial to implement an optimization over all possible unitaries in Eq. (22).

This protocol allows one to perform a forward-in-time experiment to determine the butterfly-flutter fidelity. This requires a perfect control over the system-environment space (the R space), in order to implement the correction unitary V , and a perfectly isolated ancilla space that is not itself influenced by decoherence effects or other uncontrolled dynamics. However, the correction unitary itself is, in principle, easy to implement by construction. The

predominant difficulty is how exactly to perform the maximization over $V \in \mathcal{R}$ in Eq. (22). It would be interesting to determine an efficient algorithm that could approximate this optimization.

F. Summary and discussion

We now restate the hierarchy of conditions for quantum chaos. For two butterfly flutters, with Choi states $|\vec{x}\rangle$ and $|\vec{y}\rangle$, we call a process $|\Upsilon\rangle$ chaotic if:

(C1) (*Perturbation orthogonalizes future state.*) The final state on R should be strongly sensitive to butterflies on B :

$$|\langle \Upsilon_{R|\vec{x}} | \Upsilon_{R|\vec{y}} \rangle|^2 \approx 0, \quad (31)$$

or, equivalently (Proposition 1),

$$S(\Upsilon_B) \sim \log(d_B). \quad (32)$$

(C2) (*Scrambling as volume-law entanglement.*) Butterflies on B should affect a large portion of the final state on R :

$$S(\Upsilon_{B_1 R_1}) \sim \log(d_{B_1} d_{R_1}), \quad (33)$$

for appropriate choices of $\mathcal{H}_{R_1} \subset \mathcal{H}_R$ and $\mathcal{H}_{B_1} \subseteq \mathcal{H}_B$.

(C3) (*Complexity of sensitivity.*) Different butterflies on B should lead to different enough states on R , as measured by the butterfly-flutter fidelity:

$$\zeta(\Upsilon) = \sup_{V \in \mathcal{R}, \langle \vec{x} | \vec{y} \rangle = 0} |\langle \Upsilon_{R|\vec{x}} | V | \Upsilon_{R|\vec{y}} \rangle|^2 \approx 0 \quad (34)$$

for some defined set of bounded-complexity unitaries \mathcal{R} .

The operational criteria for quantum chaos impose several restrictions on the spatiotemporal correlation content of a process. (C1) and (C2) require that Υ is volume entangled, while (C3) further requires that the process itself must be able to dynamically generate volume-law spatiotemporal entanglement. Importantly, these criteria directly lead to a universal operational metric for quantum chaos in Eq. (22), which we have shown to be accessible in a laboratory setting.

We have then used these ideas, especially (C3), to show how quantum processes are also sensitive to initial conditions, much like their classical counterparts. This opens up the possibility of operationally defining quantum Lyapunov exponents to further close the gap between the theories of classical and quantum chaos. Finally, (C3) has the same flavor as the *complexity=volume* conjecture due to Susskind [62] (for the strengthened version of the same conjecture, also see Ref. [63]). Namely, the operational

metric for quantum chaos is concerned with the complexity of the correction unitary in Eq. (22). Our results therefore hint that quantum chaos may be key to understanding this conjecture, fitting with the common belief that black holes are maximally chaotic quantum systems [64,65]. On the other hand, the tools presented in Ref. [63] are likely applicable to the case of quantum chaos.

We show in Sec. IV D that the previous dynamical signature of the local-operator entanglement measures this single-time sensitivity, optimizing over any initial state. Further, it can be shown that OTOCs generically probe this operator entanglement [30]. The hierarchy (C1)–(C3) gives a robust understanding of why these previous diagnostics measure chaos, in terms of a future sensitivity to past local operations.

IV. CONNECTION TO PREVIOUS SIGNATURES

Our construction so far has involved a first-principles proposition of a series of conditions that mean chaos as a sensitivity to perturbation in quantum systems. We will now show how these conditions (C1)–(C3) compare to previous dynamical signatures of chaos (see the diagram of this connection in Fig. 1). The Peres-Loschmidt echo corresponds to (C1) in the many-time limit and for weak butterflies, while dynamical entropy is exactly the entanglement scaling of $|\Upsilon\rangle$ in the splitting $B : R$ and so is in some sense equivalent to the Peres-Loschmidt echo scaling according to Proposition 1. The tripartite mutual information measures spatiotemporal entanglement for a single-time butterfly and so (C2) can be seen as a multitime generalization of this measure. Finally, the local-operator space entanglement measures the required entanglement complexity of the correction unitary V , such that $\zeta(\Upsilon) = 1$ for any initial state. For a summary of these connections, see Fig. 2. In this section, we will explain these diagnostics and show each of these connections in turn. Our first-principles construction is supported by, and contains a range of, previous notions of quantum chaos from recent years, all within a single intuitive framework.

A. Peres-Loschmidt echo

The Peres-Loschmidt echo measures the sensitivity of an isolated quantum system to a weak perturbation to the dynamics [11,66]. It is equal to the deviation in fidelity between the same initial states evolving unitarily according to some Hamiltonian compared to a perturbed Hamiltonian,

$$|\langle \psi_t | \psi_t^\epsilon \rangle|^2 = |\langle \psi | e^{iHt} e^{-it(H+\epsilon T)} | \psi \rangle|^2. \quad (35)$$

This equivalently measures the distance from the initial state, when a state evolves forward in time, then evolves

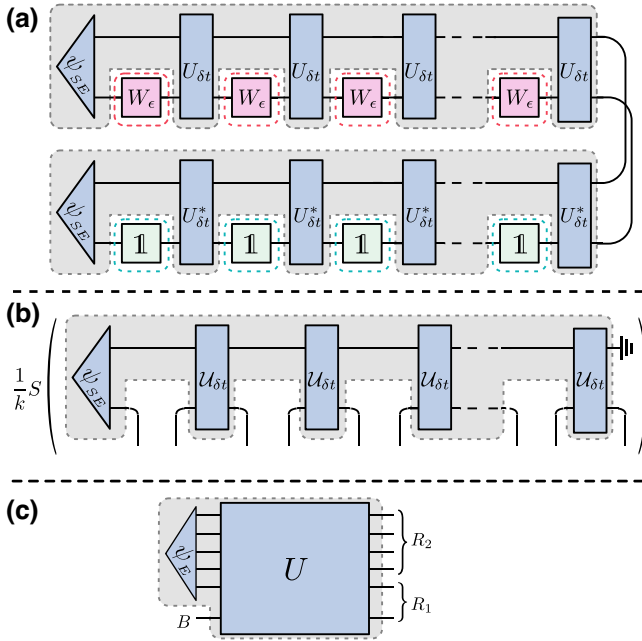


FIG. 7. The quantum process construction for the dynamical signatures: (a) Peres-Loschmidt echo, (b) dynamical entropy, and (c) tripartite mutual information. Note that the diagrams of (a) and (c) are in the pure-state representation, such that the initial state is a state vector (ket) and the boxes correspond to matrices (Latin script), while (b) is in the superoperator representation, such that the initial state is a vectorized density matrix, and the boxes represent quantum channels in the Liouville superoperator representation (calligraphic script). For further details, see Sec. II and Ref. [34].

backward in time according to imperfect evolution. Exponential decay with time is regarded heuristically to mean quantum chaos. In practice [12,67], one often needs to discretize the dynamics in order to realize the perturbation to the Hamiltonian, T . To do so, one can use the Trotter approximation of the perturbed evolution,

$$\begin{aligned} e^{-it(H+\epsilon T)} &\approx (e^{iH\delta t} e^{i\epsilon T\delta t})^k, \\ &=: (U_{\delta t} W_\epsilon)^k, \end{aligned} \quad (36)$$

where $k\delta t = t$, which is valid for large k and small δt . Then, up to Trotter error [68], the Peres-Loschmidt echo corresponds to the fidelity between two final states, given the application of k identity channels, compared to k unitaries, which are ϵ -close to the identity [see Fig. 7(a)]. From this, we can already see that the Peres-Loschmidt echo falls into the category of a fidelity between resultant states given two past butterfly flutters as in (C1) [see Eq. (17)].

In addition to the Trotterization, the key difference between our condition (C1) and the Peres-Loschmidt echo is that instead of optimal butterflies, we specify the two many-time butterfly flutters to be projections that are $(k\epsilon)$ -close. These two projections are, respectively, the Choi

states of a sequence of k weak unitaries and a sequence of k identity maps, such that

$$\begin{aligned} |\langle \bar{x} | \bar{y} \rangle| &:= |\langle W_\epsilon^{\otimes k} | \mathbb{1}^{\otimes k} \rangle| \\ &= |\langle W_\epsilon | \mathbb{1} \rangle|^k \\ &= (1 - \epsilon)^k d_S^{2k}, \end{aligned} \quad (37)$$

where we recall that $d_B = d^{2k}$. Then, for a typical volume-law process, consisting of random dynamics as described around Eq. (21) and further explored in Sec. V, under the action of any two butterflies of appropriate size we have that $\Upsilon_B \sim \mathbb{1}/d_B$, and so typically,

$$\begin{aligned} |\langle \Upsilon_{R|\bar{x}} | \Upsilon_{R|\bar{y}} \rangle|^2 &\approx \frac{|\langle \bar{x} | \mathbb{1}/d_B | \bar{y} \rangle|^2}{\langle \bar{x} | \mathbb{1}/d_B | \bar{x} \rangle \langle \bar{y} | \mathbb{1}/d_B | \bar{y} \rangle} \\ &= (1 - \epsilon)^{2k} d_B^2 (1/d_B^2) \\ &= (1 - \epsilon)^{2k} \\ &\approx e^{-2k\epsilon}, \text{ for small } \epsilon, \\ &\approx 0, \text{ for large } k. \end{aligned} \quad (38)$$

In the first line, we have used the Schmidt decomposition, as in Fig. 4(b) and Eq. (B3). For an area-law Choi state, this fidelity will be larger and will tend to scale as the leading-order Schmidt coefficient.

For a given Trotter error, time evolution corresponds to increasing k , for a constant δt and ϵ . Therefore, in Eq. (38), we can see how exponential decay with time stems from the property of entanglement structure of the Choi state $|\Upsilon\rangle$. The choice of temporally local weak unitaries is key to this exponential time decay with time.

We have shown that the Peres-Loschmidt echo can be characterized through weak many-time butterfly flutters under the first condition (C1). It should be noted that this is the weakest condition that we argue is necessary for quantum chaos. In particular, the Peres-Loschmidt echo has no extra ingredient of an correction unitary V acting on the final states as in (C3). This distinction means that while the Peres-Loschmidt echo probes a butterfly having a strong effect, it does not probe the delocalization of this effect, i.e., the scrambling. This will become apparent in Appendix E, where we investigate an example of regular dynamics that is apparently chaotic according to the Peres-Loschmidt echo.

From Proposition 1, we see that the butterfly-flutter fidelity for $V = \mathbb{1}$ is small if and only if the entanglement $S(\Upsilon_B)$ is extensive. We will now see that the quantum dynamical entropy exactly measures this quantity asymptotically with the number of perturbations k , given a novel connection to the Peres-Loschmidt echo.

B. Dynamical entropy

The quantum dynamical entropy was originally introduced as the quantum generalization of the Kolmogorov-Sinai entropy, which quantifies the asymptotic gain of information when a classical system is repeatedly measured [3, 13–15]. It measures the long-term unpredictability of a dynamical system, with positivity indicating chaoticity in the classical case. Quantum mechanically, measurement necessarily perturbs a system and comes with its own inherent unpredictability. One can account for the entropy due to a measuring device compared to the process itself [14] but a more elegant solution is to define this quantity in a device-independent way [3, 53, 69]. Indeed, classically, Kolmogorov Sinai entropy is the entropy rate of a *stochastic process*, so the natural language of the quantum version of this requires a description of quantum stochastic processes [33, 70]: precisely the process-tensor formalism detailed in Sec. II.

Formally, dynamical entropy is defined as the asymptotic gain in information when additional (measurement) steps are added to a quantum process,

$$S_{\text{Dy}}(\Upsilon) := \lim_{k \rightarrow \infty} \frac{1}{k} S(\Upsilon_{B_k}), \quad (39)$$

where $\Upsilon_{B_k} = \text{tr}_R[\Upsilon]$ is a marginal process on k time steps, meaning a process with a given (unitary) dynamical map, measured every δt seconds. We do not need to specify what measurement, as the process tensor encodes any possible measurement protocol, fulfilling precisely the role of a spatiotemporal density matrix (for details, see Sec. II). For such an asymptotic quantity to be nonzero, this strictly requires an infinite-dimensional environment. Poincaré recurrence would render any finite isolated system to have finite total entropy in the asymptotic limit. As we consider unitary dynamics on an isolated finite-dimensional quantum system, we will not take the asymptotic limit precisely. Instead, we define the k th dynamical entropy,

$$S_{\text{Dy}}^{(k)}(\Upsilon) := \frac{1}{k} S(\Upsilon_{B_k}), \quad (40)$$

where k is taken to be large but small enough such that $d_B = d_S^{2k} \ll d_E \approx d_R$. The expression in Eq. (40) is represented graphically in Fig. 7(b). From this definition and Proposition 1, we can directly see that a nonzero $S_{\text{Dy}}^{(k)}$ is sufficient for volume-law entanglement of $|\Upsilon\rangle$. We note that as the number of interventions k increases, the size of the space \mathcal{H}_B scales exponentially [see Eq. (7)].

Proposition 4.—If the dynamical entropy is nonzero, then the process $|\Upsilon\rangle$ is volume-law entangled in the splitting $B : R$ for all times.

This is apparent from the definitions and a proof is supplied in Appendix C.

This also approximately holds true if, instead, the k -dynamical entropy is considered. What is important is that

the dynamical entropy generally exhibits distinct behavior for area- versus volume-law temporally entangled processes. This simple result shows how closely the construction of dynamical entropy agrees with the first condition (C1) derived in this work, despite arriving at it from a starkly different viewpoint—that of the quantum version of the butterfly effect.

For example, the k -dynamical entropy of a typical process, given in Eq. (21), is on average maximal:

$$\begin{aligned} S_{\text{Dy}}^{(k)}(\Upsilon^{(\boxplus)}) &= \frac{S(\frac{1}{d_S^{2k}})}{k} \\ &= \frac{\log(d_S^{2k})}{k} = 2 \log(d_S). \end{aligned} \quad (41)$$

A more precise typicality bound can be found from Theorem 3.

Moreover, one can see that summing over a full basis of butterfly flutters gives a quantity proportional to this entanglement.

Proposition 5.—Consider a full basis of local unitary butterfly flutters, $\mathcal{X} = \{A_{w_1}, A_{w_2}, \dots, A_{w_k}\}^{d_B}$, where the number of operations at each time in the set is $\#w_i = d_S$ (for an example construction of this, see Appendix D). Then, the following relation holds:

$$S^{(2)}(\Upsilon_B) = -\log\left(\frac{1}{d_B^2} \left(\sum_{\vec{x} \neq \vec{y} \in \mathcal{X}} |\langle \vec{x} | \Upsilon_B | \vec{y} \rangle|^2 - d_B \right)\right), \quad (42)$$

where $S^{(2)}(\Upsilon_B)$ is the quantum 2-Rényi entropy.

This is proved in Appendix C. There is a large body of literature arguing that under certain conditions, both the Peres-Loschmidt echo [11, 12, 71, 72] and OTOCs [73–75] decay exponentially across some time regimes for chaotic systems. Given the close ties between the butterfly-flutter fidelity and other metrics that we describe in this work, it is not unreasonable to speculate that the butterfly-flutter fidelity exhibits similar behavior. Equation (C5) then forms a relation between dynamical entropy and these conjectured quantum Lyapunov exponents. This is suggestive of a kind of *quantum Pesin's theorem*, [76] although more needs to be done to understand how and when the butterfly-flutter fidelity produces an exponential decay and to refine the notion of quantum dynamical entropy.

To our knowledge, the exact connection of dynamical entropy to quantum chaos as a sensitivity to perturbation has not yet been explored in the literature; it has only been proposed as a generalization of the classical equivalent, Kolmogorov-Sinai entropy. Here, we can essentially *derive* dynamical entropy, starting from our principle (C1) and connecting it to the Peres-Loschmidt echo and other notions of chaos as a sensitivity to perturbation.

Due to the classical equivalences between Lyapunov exponents and Kolmogorov Sinai entropy, one might be

tempted to conflate quantum chaos with a nonzero dynamical entropy. This, however, only accounts for the weakest of the three conditions (C1)–(C3). Equivalently, it only allows V in the butterfly-flutter fidelity of Eq. (22) to be strictly equal to the identity. As we have already discussed in Sec. III, this is an insufficient characterization. For example, free-fermion dynamics generally exhibit an extensive dynamical entropy [53], as does dynamics consisting of SWAP gates, as we detail in Appendix E (both valid up to finite-dimension constraints). We therefore move onto the more robust conditions of quantum chaos, based around spatiotemporal entanglement (C2) and the butterfly-flutter fidelity (C3).

C. Tripartite mutual information

Here, we will show that the spatiotemporal entanglement (C2), in the single-time case, corresponds to the tripartite mutual information signature of chaos as introduced in Ref. [19], sometimes termed “strong scrambling.”

The tripartite mutual information is a measure between a subsystem of the input to a quantum channel and some bipartition of the output. Considering a single-time butterfly flutter, as in Fig. 7(c), in our language this corresponds to

$$I_3(B : R_1 : R_2) := I(B : R_1) + I(B : R_2) - I(B : R), \quad (43)$$

recalling that $\mathcal{H}_R = \mathcal{H}_{R_1} \otimes \mathcal{H}_{R_2}$, and where $I(A : B)$ is the quantum mutual information, defined as

$$I(A : B) := S(\rho_A) + S(\rho_B) - S(\rho_{AB}). \quad (44)$$

Note that this single-time butterfly flutter protocol process corresponds exactly to the setup from Ref. [19] when the initial state is separable across $S : E$. This is represented in Fig. 7(c). When the tripartite information given in Eq. (43) is near minimal, it is argued that the channel is strongly scrambling. This quantity has been connected to an average of an infinite-temperature OTOC over a complete basis of operators [19]; for a similar result, see also Proposition 5. We can in fact show directly that volume-law spatiotemporal entanglement implies strong scrambling.

Proposition 6.—If the single-intervention process $|\Upsilon\rangle$ is volume-law spatiotemporally entangled in the splitting $BR_1 : R_2$, then the corresponding channel is strongly scrambling, i.e., $I_3(B : R_1 : R_2) \approx -2 \log(d_B)$.

This is proved in Appendix C.

Given this connection, we can see that one could easily generalize the tripartite-mutual-information signature of chaos to a many-time butterfly space rather than single-time, together with some bipartition of the final pure state on \mathcal{H}_R . This may offer new insight into the sensitivity of many-body systems to multitime interventions.

We will now go on to discuss connections of the butterfly-flutter fidelity, as in (C3), with previous signatures.

D. Local-operator entanglement and OTOCs

Consider an initially local operator that evolves in time according to the Heisenberg picture,

$$X_t = U_t^\dagger X U_t. \quad (45)$$

One can compute the Choi state of this object by acting it on one half of a maximally entangled state on a doubled space, using the CJI as described in Sec. II,

$$|X_t\rangle =: X_t \otimes \mathbb{1} |\phi^+\rangle. \quad (46)$$

The entanglement of this object across some spatial bipartition is known as the local-operator entanglement and its scaling in time is considered to be a signature of chaos [16–18]. In particular, if it scales linearly with time, then the dynamics cannot be efficiently classically simulated and linear scaling is conjectured to be characteristic of nonintegrability [17, 18, 77–82].

Theorem 2.—Consider the butterfly-flutter fidelity given in Eq. (22), choosing the set of correction unitaries without volume-law entanglement, $\mathcal{R} = \mathcal{R}_{\text{MPO}}$, and the single-time butterfly flutters chosen to be the identity matrix $\mathbb{1}$ and local unitary X . Then, if for any initial state, $\zeta(\Upsilon) \approx 1$, then also

$$S(|X_t\rangle) \sim \mathcal{O}(\log(t)), \quad (47)$$

characteristic of (interacting) integrable dynamics.

This is proved in Appendix C. By the contrapositive statement of Theorem 2, we can see that if the local-operator entanglement scales linearly, the butterfly-flutter fidelity is small, i.e., chaotic according to our prescription (C3).

The local-operator entanglement is intimately related to the OTOC. In Ref. [30] it is shown the OTOC serves as a probe of local-operator entanglement, with exponential scaling of the OTOC being a strictly necessary condition for linear (chaotic) growth of local-operator entanglement. We suspect that there may be strong connections between a multitime generalization of the OTOC [25], a kind of multipoint-operator entanglement, and the volume-law spatiotemporal-entanglement structure as in (C2). We leave this for future work.

E. Discussion: Chaos and many-body phenomena

Throughout this section, we have shown how the three conditions (C1)–(C3) encapsulate some of the most common quantum chaos diagnostics studied in recent years (summarized in Fig. 2). In contrast to these other approaches, we have started with a highly intuitive principle of chaos as a sensitivity to perturbation, without appealing to classical limits (which may not be well

defined in many quantum systems) or heuristic observations. This leads to a rather direct notion of which signatures are stronger than others and a framework with which to analyze the chaoticity of a system.

We now make a few comments about how our formalism compares to others often considered in many-body physics. The setup for butterfly flutters, Definition 1, strongly resembles that of Floquet systems [83]. A Floquet Hamiltonian is a periodic time-dependent Hamiltonian, such as that produced by introducing a periodic kick to an otherwise time-independent Hamiltonian. If, in our construction, we replace the (small) butterfly flutters with strong global unitaries, they no longer function as a *small* perturbation to the process. Instead, they may change the qualitative behavior of the process, possibly creating chaos or order. For example, the quantum rotor is clearly a regular system, whereas the quantum kicked rotor is chaotic for strong enough kicks [84]. The key difference here is that a system-wide strong unitary is not classified as a butterfly flutter (as in Definition 1), as it is neither weak nor localized. Considering (C2), a strong global “perturbation” can change the entanglement structure of a process. Likewise, a strong global butterfly acting on an already chaotic process will likely lead to a similarly chaotic process.

However, this is not always the case. If a butterfly flutter acts strongly and locally on the whole system plus environment, we expect that it can break the volume-law spread of entanglement. In this case, according to the criteria (C2), the corresponding process – with a global butterfly space \mathcal{H}_B – would be trivially “non-chaotic” according to this choice of entanglement-breaking butterfly flutter. Relatedly, it would be interesting to determine the entanglement structure of systems exhibiting many-body localization (MBL) [85,86], and measurement-induced phase transitions [87,88]. MBL systems are known to be resistant to perturbation, the opposite of chaotic according to the principles underlying (C1)–(C3). While these two phenomena have previously been considered surprising, the framework presented here offers a novel path to systematically studying the mechanisms behind them. Such topics would be interesting to investigate in more detail in future work.

V. MECHANISMS FOR CHAOS

So far, in Sec. III, we have proposed a hierarchy of conditions on quantum chaos, inspired by the principle of chaos as a sensitivity to perturbation. This has culminated in the metric of the butterfly-flutter fidelity, closely connected to the spatiotemporal entanglement of the corresponding process $|\Upsilon\rangle$. Then, in Sec. IV, we have shown how this connects to and encompasses a range of existing dynamical signatures. Looking at the summary of this work (see Fig. 1), we have yet to discuss the mechanisms

of chaos on the left of this figure; the underlying properties of the dynamics that lead to chaotic phenomena in a quantum system.

We will now analyze two broad classes of dynamics and show through these that randomness typically leads to chaos. Consider dynamics that is globally random. More formally, we independently sample unitary matrices from the Haar probability measure $U_i \sim \mathbb{H}$ between each intervention in the butterfly flutter protocol given in Eq. (16). \mathbb{H} is the unique unitarily invariant measure, meaning that if any ensemble $\{U_i\}$ is distributed according to the Haar measure, then so is $\{WU_i\}$ and $\{U_iW\}$ for any unitary W . Considering such random unitaries allows one to derive strong concentration-of-measure bounds. One such famous example for quantum states says that small subsystems of large random pure states are exponentially likely to be maximally mixed [8]. Similarly, processes sampled through Haar-random evolution between interventions are highly likely to look like the completely noisy process, given a large environment dimension [59,60] (see Appendix F). By a completely noisy process, we mean that any measurements result in equal weights, corresponding to the identity matrix Choi state as in Eq. (21).

However, strictly Haar-random evolution is not entirely physical, with the full exponentially large Hilbert space not practically accessible—a “convenient illusion” [89]. On the other hand, quantum circuits with finite depth represent a far more reasonable model for realistic dynamics. Moreover, one can simulate randomness up to the first t moments using unitary design circuits. An ϵ -approximate t -design can formally be defined such that

$$\mathcal{D}(\mathbb{E}_{\mu_{\epsilon}}\{(U^\dagger)^{\otimes s}(X)U^{\otimes s}\} - \mathbb{E}_{\mathbb{H}}\{(U^\dagger)^{\otimes s}(X)U^{\otimes s}\}) \leq \epsilon,$$

for all $s \leq t$, some appropriate metric \mathcal{D} , and any observable $X \in \mathcal{H}^{\otimes s}$. In words, the s -fold channel of a t -design needs to approximately agree with perfectly Haar-random sampling. Such design circuits therefore simulate full unitary randomness but are much more akin to real physical models. For example, an ϵ -approximate 2-design can be generated efficiently from two-qubit gates only in polynomial time [90]. This is equivalent to a model of two different two-body interactions occurring randomly in a system [60].

We will now give concentration-of-measure bounds both for unitary designs and for full Haar-random evolution. We will see that sampling from these random dynamics is highly likely to produce a process with volume-law spatiotemporal entanglement, as in (C2).

Theorem 3.—(Most Processes Are Chaotic) Consider a pure process $|\Upsilon\rangle$ generated by random dynamics, either entirely Haar random, denoted by \mathbb{H} , or according to an ϵ -approximate t -design, denoted by $\mu_{\epsilon-t}$. Then, for any $R_1 \subset$

R such that $d_{R_1} \approx d_S$, and for any $\delta > 0$ and $0 < m < t/4$,

$$\mathbb{P}_{U_i \sim \mu} \left\{ \log(d_{BR_1}) - S^{(2)}(\Upsilon_{BR_1}) \geq \mathcal{J}_\mu(\delta) \right\} \leq \mathcal{G}_\mu(\delta). \quad (48)$$

where for a process generated from independent Haar-random evolution,

$$\begin{aligned} \mathcal{J}_\mathbb{H}(\delta) &= \log(d_{BR_1}(\mathcal{B} + \delta) + 1) \approx d_{BR_1} \left(\frac{1}{d_R} + \delta \right), \text{ and} \\ \mathcal{G}_\mathbb{H}(\delta) &= \exp[-C\delta^2] \approx \exp \left[-\frac{(k+1)d_R}{8d_B} \delta^2 \right], \end{aligned} \quad (49)$$

while for that generated from an ϵ -approximate unitary t -design,

$$\begin{aligned} \mathcal{J}_{\mu_{\epsilon-t}}(\delta) &= \log(d_{BR_1}\delta + 1) \approx d_{BR_1}\delta, \text{ and} \\ \mathcal{G}_{\mu_{\epsilon-t}}(\delta) &= \frac{\mathcal{F}(d_B, d_R, m, t, \epsilon)}{\delta^m}. \end{aligned} \quad (50)$$

The exact definitions of \mathcal{B} , \mathcal{C} , and \mathcal{F} are provided in Eqs. (F3), (F8) and (F10), respectively. The approximations in Eqs. (F2) and (F3) are valid for $d_R \gg d_B \gg 1$ and for small δ .

The proof of this theorem builds on results from Refs. [59,60] and can be found in Appendix F. The result given in Eq. (F1) states that random dynamics are likely to lead to a volume-law spatiotemporal entanglement, according to a small butterfly flutter in comparison to the total isolated system. In particular, for Haar-random dynamics, Eq. (F2) indicates an exponentially small probability that a single sampling deviates strongly from maximal entanglement in the splitting $BR_1 : R_2$. Further, this result is valid for any choice of \mathcal{H}_{R_1} , given that it is small enough in comparison to the full system \mathcal{H}_R . This directly implies that random dynamics typically have volume-law spatiotemporal entanglement.

Note that the bounds given here are for the independently sampled evolution between butterfly times but we note that techniques in Ref. [59] can be used to prove similar bounds for repeated dynamics, i.e., a single sample of a unitary evolution matrix that describes all dynamics between interventions.

Similarly, random circuits yield a related bound in terms of how well they approximate a unitary design. In this case, Eq. (F3) is a polynomially small bound and in practice it can be optimized over the parameter m . The key point is that both of these probability bounds are small for $d_E \gg d_{BR_1}$.

While these concentration-of-measure bounds are for the spatiotemporal entanglement of $|\Upsilon\rangle$, similar bounds can also be proved for other dynamical signatures that derive from this, such as those considered in Sec. IV. For example, dynamical entropy is likely to be extensive

according to this result. This is immediate to see from Theorem 3 by choosing \mathcal{H}_{R_1} to be empty. This therefore means that repeated measurements of a process generated from random evolution give almost maximal information. That is, one typically only sees approximately maximally noisy measurement results.

We have shown that Haar-random evolution, as well as that generated by ϵ -approximate t -designs, constitute mechanisms that are highly likely to produce chaos. This is clearly not the only internal mechanism that causes chaotic phenomena [cf. Fig. 1(a)]. The next step will be to understand how a continuous quantum evolution, defined by time-independent Hamiltonians, can lead to chaos.

For example, the so-called Wigner-Dyson level-spacing distribution is often conflated with quantum chaos [2,5]. This is the empirical observation that if one computes the distribution between next-neighbor energy levels, it follows a characteristic form when the semiclassical limit of the Hamiltonian is chaotic. An interesting connection may be found in entanglement spectra, which can be connected to a sense of irreversibility of the dynamics [91]. Another example is the ETH, which proposes that certain ‘‘physical’’ observables look thermal according to individual eigenstates of certain Hamiltonians. Often one calls such Hamiltonians chaotic and the ETH leads to a deterministic (pure-state) foundation of statistical mechanics results.

It would be interesting to determine how (if) these mechanisms lead to volume-law spatiotemporal entanglement within a process, to prove that they are mechanisms of chaos as in Fig. 1. Indeed, such a connection would firmly cement quantum chaos as a foundational deterministic principle underlying statistical mechanics, in perfect analogy with the classical case. Volume-law entanglement of eigenstates is already a key feature of the strong ETH. In addition, for a wide range of specific Hamiltonian classes, Ref. [92] determines that volume-law entanglement is highly typical. In this context, a key question will be how (many-body) quantum scars play into this, i.e., when some eigenstates of an apparently chaotic Hamiltonian do not satisfy the ETH. Such eigenstates can have different entanglement scaling [93,94].

Finally, the typicality bounds presented here have foundational implications regarding the prevalence of Markovianity in nature, which we now discuss in our concluding remarks.

VI. CONCLUSIONS

Starting from a theory-independent notion of chaos as the butterfly effect, in this work we have identified a series of conditions on quantum chaos (Sec. III), with the strongest being measured by the butterfly-flutter fidelity, shown that these proposed conditions generalize and hence unify a range of previous diagnostics (Sec. IV), and shown

how a number of mechanisms lead to quantum chaos (Sec. V). This framework is summarized in Fig. 1.

The results of Refs. [59,60] state that processes generated from random dynamics are highly likely to be almost Markovian, for large enough systems. Paradoxically, Theorem 3 states that perturbations in such processes have a strong impact in the environment. That is, most random processes are chaotic. To make sense of this, note that Markovianity is with respect to a restricted measurement space, often taken to be small. Then, when a process is highly chaotic, a butterfly impacts the future pure state in such a strong and nonlocal way that for any small subsystem it looks entirely noisy and hence Markovian on this future measurement space. Given that, in nature, chaos is the rule, not the exception, this helps to address the fundamental question of why Markovian phenomena are so prevalent in nature [40,41,44,59,60]: chaotic processes on large systems look Markovian with respect to interventions on a much smaller subsystem. We anticipate that this may be a key factor in understanding the emergence of thermalization from underlying quantum theory; in particular, the necessary loss of memory in the process of thermalization. It would be interesting to investigate this further in a future work.

This is related to Refs. [95,96], where it is shown that states that are too entangled—i.e., most states in the full Hilbert space—are not useful for measurement-based quantum computation. For such states that are too entangled, one can replace the local statistics with “coin flipping”—purely classical stochasticity. It is, however, very difficult to produce large highly entangled states. Usefulness is not necessarily proportional to the resources required to create a state. Our results in Sec. V are a spatiotemporal version of this. Most processes are so chaotic that future measurements statistics constitute purely classical noise. What is needed, then, to have complex, quantum non-Markovian phenomena? We propose that it is “between order and chaos” where these interesting processes lie [97]. This would correspond to processes with sub-volume-law (logarithmic) spatiotemporal-entanglement scaling. This is intrinsically tied to criticality in the spatial setting, and the multiscale entanglement renormalization ansatz (MERA) tensor network [98]. Current research explores a process-tensor ansatz, inspired by MERA, structurally exhibiting long-range (polynomially decaying) temporal correlations [99].

A relevant problem that we have not tackled in this work is the question of how (if) classical chaos emerges from quantum chaos in some limit. While, historically, this has been the main motivation for understanding quantum chaos [2,4,5], here we have developed a genuinely quantum notion of chaos, of interest for the wide range of phenomena and modern experiments in many-body physics with no classical analogue. It is therefore an open question how exactly to connect this to the classical

picture. Modern notions of the transition to classicality may be integral to understanding this, such as quantum Darwinism [100] or classical stochasticity arising from quantum theory [42–44]. Related to this is Ref. [101], where it is shown that circuits generated solely by Clifford gates, or doped with only a few non-Clifford gates, are not chaotic according to a generalized OTOC chaos signature. It would be interesting to check what kind of entanglement structure a (doped) Clifford circuit has, i.e., whether this statement is consistent with the structure of chaos that we have revealed in this work. This would have implications regarding whether any chaotic quantum process, satisfying the strongest condition (C3), can be simulated classically.

It is difficult to directly convert from classical to quantum chaos, due to the linearity of isolated quantum mechanics. The novelty of our approach is that it treats chaos itself as a primitive concept, independent of whether we adopt a classical or quantum formalism. Classically, this reduces to a nonlinearity of the dynamics in phase space. On the quantum side of things, we have shown that the spatiotemporal-entanglement structure directly satisfies this principle: perturb a small part of a system in the past and see a complex nonlocal effect in the future. From this realization, we have shown that previous diagnostics fit perfectly within this framework. Further, one can systematically compare our framework with any other quantum chaos diagnostic and use the new metrics to tackle a wide range of relevant problems in the field of many-body physics.

ACKNOWLEDGMENTS

We thank S. Singh for several technical discussions. K.M. thanks A. Gorecka for conversations that distilled some key ideas. N.D. is supported by an Australian Government Research Training Program Scholarship and the Monash Graduate Excellence Scholarship. K.M. acknowledges support from the Australian Research Council Future Fellowship FT160100073, Discovery Projects DP210100597 and DP220101793, and the International Quantum U Tech Accelerator award FA9550-21-1-0023 by the U.S. Air Force Research Laboratory.

APPENDIX A: THE PROCESS TENSOR

Here, we supplement the details of the background given in Sec. II, in order to describe how the process tensor, a familiar object in open quantum systems, can be derived from the pure process tensor $|\Upsilon\rangle$. In summary, the process tensor Υ_B corresponds to the reduced generally mixed-state description of the pure process $|\Upsilon\rangle$, when the final state on the space \mathcal{H}_R is traced over at the end.

Measurement is necessarily invasive in quantum mechanics. Therefore, to construct such a multitime description, we need to represent quantum measurements

in a way that includes the resultant state. Arbitrary interventions are defined by the action on \mathcal{H}_S by external *instruments*, which mathematically are trace nonincreasing, completely positive (CP) and time-independent maps, \mathcal{A} . If an instrument is also trace preserving (TP), then it is deterministic; e.g., a unitary map or a complete measurement [a positive operator-valued measure (POVM)]. If an instrument is trace decreasing, then it is nondeterministic; e.g., a particular measurement result. The trace of the outgoing state corresponds to the probability of this outcome occurring out of a complete measurement described by the set $\mathcal{J} = \{\mathcal{A}_{x_i}\}$,

$$\mathbb{P}(x_j|\mathcal{J}) = \text{tr}[\rho'] := \text{tr}[\mathcal{A}_{x_j}(\rho)]. \quad (\text{A1})$$

Note that in this work, calligraphic font Latin letters are generally used for such superoperators—i.e., a map of a (density) operator—while standard-font uppercase Latin or lowercase Greek letters are used for operators (matrices).

Similarly, for multiple consecutive interactions of a single quantum system at different times, the (in general, subnormalized) outgoing state is

$$\rho' = \text{tr}_E[\mathcal{U}_k \mathcal{A}_{x_k} \mathcal{U}_{k-1} \dots \mathcal{U}_1 \mathcal{A}_{x_1}(\rho(t_0))], \quad (\text{A2})$$

where $\mathcal{U}_j(\sigma) := e^{-iH(t_j-t_{j-1})}\sigma e^{iH(t_j-t_{j-1})}$ is the unitary superoperator describing the evolution of the dilated system environment ($\mathcal{H}_S \otimes \mathcal{H}_E$) and the trace is the partial trace over the environment (\mathcal{H}_E). For nondeterministic instruments, the trace of this final state gives the probability of measuring a sequence of outcomes x_1, x_2, \dots, x_k .

For rank-1 instruments as considered throughout this work, $\mathcal{A}_{x_i}(\cdot) = A_{x_i}(\cdot)A_{x_i}^\dagger$, where A_{x_i} are defined as in Eq. (3). That is, by rank-1 we mean that there is only a single Kraus operator for the CP map.

From $|\Upsilon\rangle$ in Eq. (5), one can define the reduced state only on the “butterfly space” of interventions B ,

$$\Upsilon_B := \text{tr}_R[|\Upsilon\rangle\langle\Upsilon|]. \quad (\text{A3})$$

Υ_B is called a process tensor [31–33] (also called a “quantum comb” [35,102] or “process matrix” [37,103]), and is used in, e.g., determining exact unambiguous multitime properties of open quantum systems. For one, it admits a multitime Born rule [102,104],

$$\mathbb{P}(x_k, \dots, x_1 | \mathcal{J}_k, \dots, \mathcal{J}_1) = \text{tr}[\rho'] =: \text{tr}[\Upsilon_B \mathbf{A}_x^\top], \quad (\text{A4})$$

where we have recalled the definition of the outgoing reduced state ρ' in Eq. (A2) and defined the instrument tensor \mathbf{A}_x^\top , equal to $|\vec{x}\rangle\langle\vec{x}|$, for time-local rank-1 instruments. It is not relevant here to define \mathbf{A}_x^\top in full generality (for more details, see, e.g., Ref. [33]).

Regarding normalization of the process tensor, and of instruments, note that to get well-defined probabilities in

the generalized Born rule of Eq. (A4), we take the instruments to be supernormalized and the process to be normalized. For example, a sequence of unitary maps should give unit probability for any process tensor Υ_B . This is immediate to check for, e.g., the maximally noisy process, which has a uniformly mixed reduced Choi state on \mathcal{H}_B ,

$$\text{tr}[\mathbf{U}_k^\top \Upsilon_B^{(\text{HD})}] = \frac{1}{d_S^{2k}} \text{tr}[\mathbf{U}_k] \stackrel{!}{=} 1. \quad (\text{A5})$$

This locally noisy process is relevant to this work: see the discussion around Eq. (21) and see Sec. V.

APPENDIX B: PROOF OF RESULTS FROM SEC. III

Here, we restate all of the formal results from Sec. III, together with a proof for each.

Proposition 1.—For any two orthogonal butterflies, one obtains (approximately) orthogonal final states on \mathcal{H}_R if and only if $|\Upsilon\rangle$ is (approximately) maximally entangled across the bipartition $B : R$.

Proof.—Assume that $|\vec{x}\rangle$ and $|\vec{y}\rangle$ are the Choi states of two multitime butterflies, with $\langle\vec{x}|\vec{y}\rangle = 0$. First, assume that $|\langle\Upsilon_{R|\vec{x}}|\Upsilon_{R|\vec{y}}\rangle|^2 = \epsilon \approx 0$. Then,

$$|\langle\Upsilon_{R|\vec{x}}|\Upsilon_{R|\vec{y}}\rangle|^2 = |\text{tr}_R[\langle\vec{y}|\Upsilon_{BR}\rangle\langle\Upsilon_{BR}|\vec{x}\rangle]|^2 \quad (\text{B1})$$

$$= |\langle\vec{y}|\Upsilon_B|\vec{x}\rangle|^2 = \epsilon, \quad (\text{B2})$$

given that $|\vec{x}\rangle$ and $|\vec{y}\rangle$ are projections on the butterfly space alone. Given that $|\Upsilon\rangle$ is a pure state, here we have used its Schmidt decomposition as in Eq. (12),

$$\begin{aligned} \langle\Upsilon|\vec{x}\rangle\langle\vec{y}|\Upsilon\rangle &= \sum_i \lambda_i \langle\Upsilon_B^{(\alpha_i)}|\langle\Upsilon_R^{(\beta_i)}|(|\vec{x}\rangle_B\langle\vec{y}|_B) \\ &\times \sum_j \lambda_j^* |\Upsilon_B^{(\alpha_j)}\rangle|\Upsilon_R^{(\beta_j)}\rangle \\ &= \sum_i |\lambda_i|^2 \langle\vec{y}|\Upsilon_B^{(\alpha_i)}\rangle\langle\Upsilon_B^{(\alpha_i)}|\vec{x}\rangle \\ &= \langle\vec{y}|\Upsilon_B|\vec{x}\rangle. \end{aligned} \quad (\text{B3})$$

Now, if this is true for any orthogonal butterflies $|x\rangle$ and $|y\rangle$, the only solution to Eq. (B2) is if $\Upsilon_B \propto \mathbb{1} + \epsilon\Omega$, where Ω is traceless with bounded operator norm, such that $\|\epsilon\Omega\| \leq \epsilon$. In the other direction, if $|\Upsilon_{BR}\rangle$ is approximately maximally entangled, then $\Upsilon_B = \mathbb{1} + \epsilon\Omega$ and so

$$|\langle\vec{y}|\Upsilon_B|\vec{x}\rangle|^2 = |\langle\vec{y}|\mathbb{1} + \epsilon\Omega|\vec{x}\rangle|^2 = \mathcal{O}(\epsilon^2) \approx 0. \quad (\text{B4})$$

Theorem 1.—(Random Butterflies Are Likely to Detect Spatiotemporal Entanglement) For a Haar-random choice of orthogonal butterflies $\mathcal{X} = \{|\vec{x}\rangle, |\vec{y}\rangle\}$ across the combined space $\mathcal{H}_B \otimes \mathcal{H}_{R_1}$ for any choice of space \mathcal{H}_{R_1} , the

fidelity of the final state is likely to be sensitive to the volume-law property of $|\Upsilon\rangle$. In particular, for $\delta > 0$,

$$\mathbb{P}_{\mathcal{X} \sim \mathbb{H}} \left\{ |\langle \Upsilon_{R_2|\vec{x}} | \Upsilon_{R_2|\vec{y}} \rangle|^2 \geq \delta \right\} \lesssim \frac{\text{tr}[\Upsilon_{BR_1}^2] - 1/(d_{BR_1})}{\delta}, \quad (19)$$

where $d_{BR_1} = d_B d_{R_1}$. This inequality is slightly approximated for large $d_{BR_1}^2$, such that $d_{BR_1}^2 \pm 1 \approx d_{BR_1}^2$.

Proof.—From the Schmidt decomposition in the splitting $BR_1 : R_2$, the analogue of Eq. (B3), one can equivalently write

$$|\langle \vec{y} | \Upsilon_{BR_1} | \vec{x} \rangle|^2 = |\langle \Upsilon_{R_2|\vec{x}} | \Upsilon_{R_2|\vec{y}} \rangle|^2. \quad (B5)$$

We will then use the following result, which we prove below using an application of Weingarten calculus. For the Haar-random sampling of two orthogonal projections $\{|\vec{x}\rangle, |\vec{y}\rangle\}$, the expectation value is

$$\begin{aligned} \mathbb{E}_{\mathcal{X} \sim \mathbb{H}} \left\{ |\langle \vec{y} | \Upsilon_{BR_1} | \vec{x} \rangle|^2 \right\}_{\vec{x} \perp \vec{y}} &= \frac{d_{BR_1}^2 (\text{tr}[\Upsilon_{BR_1}^2] - 1/d_{BR_1})}{d_{BR_1}^2 - 1} \\ &\approx \text{tr}[\Upsilon_{BR_1}^2] - 1/d_{BR_1}, \end{aligned} \quad (B6)$$

where we take $d_{BR_1}^2 - 1 \approx d_{BR_1}^2$ in the second line.

Two Haar-random orthogonal states $\{|\vec{x}\rangle, |\vec{y}\rangle\}_{\mathbb{H}}$ can be generated from any other, e.g., computational, orthogonal states $\{|0\rangle, |1\rangle\}$, given a random unitary matrix $U \in \mathcal{H}$, by identifying $|\vec{x}\rangle = U|0\rangle$ and $|\vec{y}\rangle = U|1\rangle$. Define $\Phi_{\mathbb{H}}^{(2)}(A)$ to be the twofold average of the tensor $A \in \mathcal{H} \otimes \mathcal{H}$. We may use Weingarten calculus to compute it explicitly [25]:

$$\begin{aligned} \Phi_{\mathbb{H}}^{(2)}(A) &:= \int dUU \otimes U(A)U^\dagger \otimes U^\dagger \\ &= \frac{1}{d^2 - 1} \left(\mathbb{1} \text{tr}[A] + \mathbb{S} \text{tr}[SA] - \frac{1}{d} \mathbb{S} \text{tr}[A] - \frac{1}{d} \mathbb{1} \text{tr}[SA] \right), \end{aligned} \quad (B7)$$

where \mathbb{S} is the SWAP operation. By choosing $A \equiv \Upsilon_{BR_1} \otimes \Upsilon_{BR_1}$, we can rewrite the left-hand side of Eq. (B6) as

$$\begin{aligned} LHS &= \int dU_{\mathbb{H}} \langle \vec{x} | U \Upsilon_{BR_1} U^\dagger | \vec{y} \rangle \langle \vec{y} | U \Upsilon_{BR_1} U^\dagger | \vec{x} \rangle \\ &= \langle \vec{x} | \langle \vec{y} | \left(\int dU_{\mathbb{H}} U^{\otimes 2} (\Upsilon_{BR_1} \otimes \Upsilon_{BR_1}) U^{\dagger \otimes 2} \right) | \vec{y} \rangle | \vec{x} \rangle \\ &= \langle \vec{x} | \langle \vec{y} | \Phi_{\mathbb{H}}^{(2)}(\Upsilon_{BR_1} \otimes \Upsilon_{BR_1}) | \vec{y} \rangle | \vec{x} \rangle \\ &= \langle \vec{x} | \langle \vec{y} | \left(\frac{1}{d_{BR_1}^2 - 1} \left(\mathbb{1} \text{tr}[\Upsilon_{BR_1} \otimes \Upsilon_{BR_1}] \right. \right. \right. \\ &\quad \left. \left. + \mathbb{S} \text{tr}[\mathbb{S}(\Upsilon_{BR_1} \otimes \Upsilon_{BR_1})] - \frac{1}{d_{BR_1}} \mathbb{S} \text{tr}[\Upsilon_{BR_1} \otimes \Upsilon_{BR_1}] \right. \right. \\ &\quad \left. \left. - \frac{1}{d_{BR_1}} \mathbb{1} \text{tr}[\mathbb{S}(\Upsilon_{BR_1} \otimes \Upsilon_{BR_1})] \right) | \vec{y} \rangle | \vec{x} \rangle. \end{aligned} \quad (B8)$$

For the first trace in this equation, we can directly evaluate

$$\text{tr}[\Upsilon_{BR_1} \otimes \Upsilon_{BR_1}] = \text{tr}[\Upsilon_{BR_1}]^2 = 1. \quad (B9)$$

For the second trace,

$$\text{tr}[\mathbb{S}(\Upsilon_{BR_1} \otimes \Upsilon_{BR_1})] = \text{tr}(\Upsilon_{BR_1}^2). \quad (B10)$$

Then, by the orthogonality of the butterflies, $\langle \vec{x} | \langle \vec{y} | \mathbb{1} | \vec{y} \rangle | \vec{x} \rangle = 0$, while $\langle \vec{x} | \langle \vec{y} | \mathbb{S} | \vec{y} \rangle | \vec{x} \rangle = d_{BR_1}^2$, and so only the second and third terms in the final line of Eq. (B8) survive. Using this, we arrive at Eq. (B6).

We will now use this to prove Theorem 1. We can directly apply Eq. (B6) to Markov's inequality [105],

$$\begin{aligned} \mathbb{P}_{\mathcal{X} \sim \mathbb{H}} \left\{ |\langle \Upsilon_{R_2|\vec{x}} | \Upsilon_{R_2|\vec{y}} \rangle|^2 \geq \delta \right\} &= \mathbb{P} \left\{ |\langle \vec{y} | \Upsilon_{BR_1} | \vec{x} \rangle|^2 \geq \delta \right\} \\ &\leq \frac{\mathbb{E}_{\mathcal{X} \sim \mathbb{H}} \left\{ |\langle \vec{y} | \Upsilon_{BR_1} | \vec{x} \rangle|^2 \right\}}{\delta} \\ &\approx \frac{\text{tr}[\Upsilon_{BR_1}^2] - 1/(d_{BR_1})}{\delta}. \end{aligned} \quad (B11)$$

■

Proposition 2.—If the butterfly-flutter fidelity given in Eq. (22) is small, $\zeta \approx 0$, then the process $|\Upsilon\rangle$ has volume-law spatiotemporal entanglement.

Proof.—We will prove this via the contrapositive statement. Assume that $|\Upsilon\rangle$ has area-law spatiotemporal entanglement. Then, the conditional states $|\Upsilon_{R|\vec{x}}\rangle$ and $|\Upsilon_{R|\vec{y}}\rangle$ can be represented efficiently by an MPS. Then, they can be prepared from an auxiliary product state $|\psi_0\rangle$ using efficient unitaries $V_{\vec{x}}$ and $V_{\vec{y}}$,

$$|\Upsilon_{R|\vec{x}}\rangle = V_{\vec{x}} |\psi_0\rangle \quad \text{and} \quad |\Upsilon_{R|\vec{y}}\rangle = V_{\vec{y}} |\psi_0\rangle, \quad (B12)$$

i.e., both $V_{\vec{x}}$ and $V_{\vec{y}}$ have an MPO representation with a constant bond dimension. It directly follows that for $V = V_{\vec{x}}^\dagger V_{\vec{y}} \in \mathcal{R}_{\text{MPO}}$,

$$\zeta(\Upsilon) = 1. \quad (B13)$$

■

Proposition 3.—If the butterfly-flutter fidelity (22) is not small (nonchaotic), $\zeta \approx 1$, but the process $|\Upsilon\rangle$ has volume-law spatiotemporal entanglement, the process can be written in terms of simple dynamics with a volume-law entangled initial state.

Proof.—Consider that the butterfly-flutter fidelity is $\zeta \approx 1$, for any two butterflies with Choi states $|\vec{x}_i\rangle$ and $|\vec{x}_j\rangle$ from some basis of butterflies $\{|\vec{x}_i\rangle\}_{i=1}^{d_B^2}$. This means that

a simple (low-depth) unitary V_{ij} in Eq. (22) approximately “corrects” the final states,

$$|\langle \Upsilon_{R|\vec{x}_i} | V_{ij} | \Upsilon_{R|\vec{x}_j} \rangle|^2 \approx 1, \quad (\text{B14})$$

where, as usual, we define a simple unitary as one with an efficient MPO representation, such that it cannot create volume-law entanglement from an area-law state. Now assume that $|\Upsilon\rangle$ is volume-law spatiotemporally entangled. In particular, this means that the final states $|\Upsilon_{R|\vec{x}_i}\rangle$ and $|\Upsilon_{R|\vec{x}_j}\rangle$ are both volume-law entangled quantum states. As $\Upsilon_{R|\vec{x}_i}$ and $\Upsilon_{R|\vec{x}_j}$ are connected via a simple circuit, we can write each of them in terms of some intermediate state

$$|\Upsilon_{R|\vec{x}_i}\rangle = V_i |R_0\rangle, \quad (\text{B15})$$

where V_i is a simple unitary but $|R_0\rangle$ is volume-law entangled. As this is true for any $|\vec{x}\rangle \in \{|\vec{x}_i\rangle\}_{i=1}^{d_B^2}$, this means that the full purified process can be written as

$$|\Upsilon\rangle = \sum_m \lambda_m (\mathbb{1}_B \otimes V_m) |B_m R_0\rangle \quad (\text{B16})$$

$$= \sum_m \lambda_m (|B_m\rangle \langle B_m| \otimes V_m) |B_0 R_0\rangle, \quad (\text{B17})$$

where, by gauge freedom, $|B_0 R_0\rangle$ is the initial state of the process [106]. However, $\sum_m \lambda_m (|B_m\rangle \langle B_m| \otimes V_m)$ is simple dynamics, in that it can be simulated efficiently with an MPO. ■

APPENDIX C: PROOFS FROM SEC. IV

Proposition 4.—If the dynamical entropy is nonzero, then the process $|\Upsilon\rangle$ is volume-law entangled in the splitting $B : R$ for all times.

Proof.—For a given bond dimension χ of a process $|\Upsilon\rangle$, in the bipartition $B : R$, the entropy of a reduced state is upper bounded by that of a uniform eigenvalue distribution,

$$S(\Upsilon_B) \leq - \sum_{i=1}^{\chi} \frac{1}{\chi} \log\left(\frac{1}{\chi}\right) = \log(\chi). \quad (\text{C1})$$

Then, recalling the characteristic scaling of the bond dimension for different entanglement classes (see Sec. II), for large k , $S(\Upsilon)$ is bounded by

$$S_{\text{Dy}}(\Upsilon_B^{(\text{vol})}) \leq \lim_{k \rightarrow \infty} \frac{\log(d_S^{2k})}{k} = 2 \log(d_S) \quad (\text{C2})$$

for volume-law entanglement scaling. Otherwise, for area-law and sub-volume-law, respectively,

$$S(\Upsilon_B^{(\text{area})}) \leq \lim_{k \rightarrow \infty} \frac{\log(D)}{k} = 0, \quad \text{and} \quad (\text{C3})$$

$$S(\Upsilon_B^{(\text{subvol})}) \leq \lim_{k \rightarrow \infty} \frac{\log(d_S^{\log(k)})}{k} = 0, \quad (\text{C4})$$

where the second limit is computed via L’Hôpital’s rule. Hence $S(\Upsilon_B)$ can only be nonzero for a volume-law entangled process. ■

Proposition 5.—Consider a full basis of local unitary butterfly flutters, $\mathcal{X} = \{A_{w_1}, A_{w_2}, \dots, A_{w_k}\}^{d_B}$, where the number of operations at each time in the set is $\#w_i = d_S$ (for an example construction of this, see Appendix D). Then, the following relation holds:

$$S^{(2)}(\Upsilon_B) = - \log \left(\frac{1}{d_B^2} \left(\sum_{\vec{x} \neq \vec{y} \in \mathcal{X}} | \langle \vec{x} | \Upsilon_B | \vec{y} \rangle |^2 - d_B \right) \right), \quad (\text{42})$$

where $S^{(2)}(\Upsilon_B)$ is the quantum 2-Rényi entropy.

Proof.—From the definition of the quantum 2-Rényi entropy,

$$\begin{aligned} S^{(2)}(\Upsilon_B) &= - \log(\text{tr}[\Upsilon_B^2]) \\ &= - \log \left(\frac{1}{d_B^2} \sum_{\vec{x}, \vec{y}} | \langle \vec{x} | \Upsilon_B | \vec{y} \rangle |^2 \right), \end{aligned} \quad (\text{C5})$$

where we have taken into account the supernormalization of instruments as in Eq. (11). Assuming that the butterfly flutters are unitary, $| \langle \vec{x} | \Upsilon_B | \vec{y} \rangle |^2 = 1$, and so

$$\begin{aligned} S^{(2)}(\Upsilon_B) &= - \log \left(\frac{1}{d_B^2} \sum_{\vec{x} \neq \vec{y}} | \langle \vec{x} | \Upsilon_B | \vec{y} \rangle |^2 \right. \\ &\quad \left. - \sum_{\vec{x}} | \langle \vec{x} | \Upsilon_B | \vec{x} \rangle |^2 \right) \\ &= - \log \left(\frac{1}{d_B^2} \left(\sum_{\vec{x} \neq \vec{y}} | \langle \vec{x} | \Upsilon_B | \vec{y} \rangle |^2 - d_B \right) \right). \end{aligned} \quad (\text{C6})$$

■
Proposition 6.—If the single-intervention process $|\Upsilon\rangle$ is volume-law spatiotemporally entangled in the splitting $BR_1 : R_2$, then the corresponding channel is strongly scrambling, i.e., $I_3(B : R_1 : R_2) \approx -2 \log(d_B)$.

Proof.—Assuming that $|\Upsilon\rangle$ is volume-law entangled, then $S(\Upsilon_B) \approx \log(d_B)$, $S(\Upsilon_{R_1}) \approx d_{R_1}$, and, in particular, $I(B : R_1) = I(B : R_2) \approx 0$. Then, from the definition of

quantum mutual information, we have that

$$\begin{aligned}
I_3(B : R_1 : R_2) &= I(B : R_1) + I(B : R_2) - I(B : R) \\
&\approx -I(B : R) \\
&= -S(\Upsilon_B) - S(\Upsilon_R) + S(\Upsilon_{BR}) \\
&\approx -2 \log(d_B), \tag{C7}
\end{aligned}$$

where we have used that $S(\Upsilon_{BR}) = 0$, as it is an isolated system, and that $S(\Upsilon_B) = S(\Upsilon_R) = \log(d_B)$, given that $d_B < d_R$ and that, for unitary dynamics, information is preserved for a single-step process. ■

Theorem 2.—Consider the butterfly-flutter fidelity given in Eq. (22), choosing the set of correction unitaries without volume-law entanglement, $\mathcal{R} = \mathcal{R}_{\text{MPO}}$, and the single-time butterfly flutters chosen to be the identity matrix $\mathbb{1}$ and local unitary X . Then, if for any initial state, $\zeta(\Upsilon) \approx 1$, then also

$$S(|X_t\rangle) \sim \mathcal{O}(\log(t)), \tag{47}$$

characteristic of (interacting) integrable dynamics.

Proof.—For the two butterfly flutters X and $\mathbb{1}$, the butterfly-flutter fidelity in Eq. (22) is equal to

$$\zeta(\Upsilon) := \text{tr}[VU|\psi\rangle\langle\psi|X^\dagger U^\dagger]. \tag{C8}$$

If we enforce that $\zeta(\Upsilon) \stackrel{\dagger}{=} 1$ for any initial state, then this means that

$$X^\dagger U^\dagger VU \stackrel{\dagger}{=} \mathbb{1}, \tag{C9}$$

which directly implies that the correction unitary is equal to

$$V = UXU^\dagger = X_{-t}.$$

Now, as we have assumed that $V \in \mathcal{R}_{\text{MPO}}$, this means that as an efficient MPO, X_{-t} has bond dimensions that scale at most logarithmically, for any t . This also means that the MPO representation of X_t has restricted bonds. Finally, this equivalently implies that the Choi state of the operator has a restricted bond dimension, for any t .

$$S(|X_t\rangle) \sim \mathcal{O}(\log(t)). \tag{C10}$$

■

APPENDIX D: CONSTRUCTION OF A LOCAL BASIS OF MULTITIME UNITARY INSTRUMENTS

To construct a basis of unitary butterflies, one can carry out the following procedure:

- (1) Choose any orthonormal basis of unitary matrices $\{\sigma_i^{(\ell)}\}_{i=1}^{d_S^2}$ for each time t_ℓ :

$$\text{tr}[\sigma_i^{(\ell)} \sigma_j^{(\ell)}] = d_S \delta_{ij}. \tag{D1}$$

For example, this could be the generalized Pauli matrices [107]. These are taken to act on the system Hilbert space $\mathcal{H}_{S(t_\ell)}$.

- (2) Using single-time CJI (see Sec. II and Fig. 3), map these operators to states by having them act on half of a maximally entangled state on the doubled space $\mathcal{H}_{S(t_\ell)} \otimes \mathcal{H}_{S(t_\ell)'}$:

$$|x_i^{(\ell)}\rangle := (\sigma_i^{(\ell)} \otimes \mathbb{1}) |\phi^+\rangle_{S(t_\ell)S'(t_\ell)}. \tag{D2}$$

The orthonormality condition in Eq. (D1) carries over to this representation:

$$\langle x_i^{(\ell)} | x_j^{(\ell)} \rangle = d_S \delta_{ij}. \tag{D3}$$

- (3) Do this for every time to arrive at a full basis for the butterfly space $\mathcal{H}_B \equiv \mathcal{H}_{S(t_k)}^{\text{io}} \otimes \mathcal{H}_{S(t_{k-1})}^{\text{io}} \cdots \otimes \mathcal{H}_{S(t_2)}^{\text{io}} \otimes \mathcal{H}_{S(t_1)}^{\text{io}}$, together with some portion of the final state, \mathcal{H}_{R_1} :

$$\begin{aligned}
&\{|\vec{x}_i'\rangle\}_i^{d_{BR_1}^2} \\
&:= \left\{ |x_{i_0}^{(0)}\rangle \otimes |x_{i_1}^{(1)}\rangle \otimes \cdots \otimes |x_{i_k}^{(k)}\rangle \right\}_{i_0, i_1, \dots, i_k=1}^{d_{R_1}, d_S, \dots, d_S}.
\end{aligned}$$

This basis is local in time.

APPENDIX E: THE LINDBLAD-BERNOULLI SHIFT

Here, we consider a somewhat pathological example that is not chaotic, yet looks so for many of the usual diagnostics. First proposed by Lindblad [3] as a quantum counterpart to the Bernoulli-shift classical stochastic process, the *Lindblad-Bernoulli shift* describes a discrete quantum process that cyclically permutes an n -body $\mathcal{H}_S \otimes \mathcal{H}_E$ state, together with some local unitary L on the \mathcal{H}_S state:

$$\mathcal{U}(\phi_1 \otimes \phi_2 \otimes \cdots \otimes \phi_n) = (L\phi_2 L^\dagger) \otimes \cdots \otimes \phi_n \otimes \phi_1. \tag{E1}$$

We take the total system size n to be large, compared to the number of time steps k that we will consider, such that states fed into the process are essentially “lost” to the environment. Additionally, we take the total initial $\mathcal{H}_S \otimes \mathcal{H}_E$ state to be in a product state, $|\psi\rangle_{SE} = \phi_1 \otimes \cdots \otimes \phi_n$.

Intuitively, this system is highly regular. It simply cycles through different states in a straightforward manner, without any scrambling of local information. Any information

put into the process on the system level will never return from the large environment \mathcal{H}_E . Indeed, while this process has a maximal $B : R$ entanglement (C1), it is not volume-law spatiotemporally entangled (C2) as the Choi state is a product state, which we will now show.

For a single time step, the reduced map Λ is uncorrelated with any other time step, where

$$\Lambda(\rho) := \text{tr}_E(\mathcal{U}_i(|\psi_{SE}\rangle \langle \psi_{SE}|)). \quad (\text{E2})$$

Then, by the CJI, this channel acting on one half of a maximally entangled state gives its Choi representation,

$$\Lambda_i \otimes \mathbb{1}(|\phi^+\rangle \langle \phi^+|) = L\phi_i L^\dagger \otimes \frac{\mathbb{1}}{d_S}. \quad (\text{E3})$$

Then, the total process Choi state, for $k < n$ time steps, is

$$\Upsilon^{(\text{LB})} = \bigotimes_{i=1}^k \left(L\phi_i L^\dagger \otimes \frac{\mathbb{1}}{d_S} \right). \quad (\text{E4})$$

Looking at the Peres-Loschmidt echo for this example,

$$\begin{aligned} \zeta'(\Upsilon^{(\text{LB})}, \mathcal{X}_{\text{LE}}) &= |\langle \mathcal{W}_\epsilon^{\otimes k} | \Upsilon^{(\text{LB})} | \mathbb{1}^{\otimes k} \rangle|^2 \\ &= \prod_i^k |\langle \mathcal{W}_\epsilon | L\phi_i L^\dagger \otimes \frac{\mathbb{1}}{d_S} | \mathbb{1} \rangle|^2 \\ &= \prod_i^k |\langle \phi^+ | (\mathcal{W}_\epsilon^\dagger \otimes \mathbb{1}) (L\phi_i L^\dagger \otimes \frac{\mathbb{1}}{d_S}) | \phi^+ \rangle|^2 \\ &= \prod_i^k |\text{tr}[L^\dagger \mathcal{W}_\epsilon^\dagger L \phi_i]|^2 \\ &\leq \prod_i^k |\text{tr}[L^\dagger \mathcal{W}_\epsilon^\dagger L]| |\text{tr}[\phi_i]|^2 \\ &= |\text{tr}[\mathcal{W}_\epsilon]|^{2k} = (1 - \epsilon)^{2k} d_B \approx 0, \end{aligned} \quad (\text{E5})$$

where $|\phi^+\rangle$ is the unnormalized d_S^2 -dimensional maximally entangled state on the space $\mathcal{H}_S^0 \otimes \mathcal{H}_S^i$, which is equal to the vectorized identity matrix. In the final line, we have used that for positive operators, $\text{tr}(XY) \leq \text{tr}(X) \text{tr}(Y)$, ϕ_i is a density matrix and the weakness of the unitary perturbation $|\langle \mathcal{W}_\epsilon | \mathbb{1} \rangle| = \text{tr}[\mathcal{W}_\epsilon] = (1 - \epsilon)d_S$. Recall that the prime on ζ means that we neglect any correction unitary \mathcal{H}_R , setting it to $V = \mathbb{1}$. From the smallness of Eq. (E5), we see that ζ' for the Peres-Loschmidt echo misclassifies this example as chaotic. It detects that the butterfly orthogonalizes the entire final state on \mathcal{H}_R but not that this effect scrambles throughout \mathcal{H}_R .

Adding a correction unitary V of consisting of a single layer of k entirely local gates, the full butterfly-flutter fidelity given by ζ in Eq. (22) will correctly detect the

Lindblad-Bernoulli shift as non-chaotic, with $\zeta = 1$. This is because V will act to align the part of the environment where the perturbation effect resides. For simplicity, we consider ζ , where the butterflies $|\vec{x}\rangle$ and $|\vec{y}\rangle$ correspond to complete measurements and independent preparations at each time step, inputting pure orthogonal states ψ_i^x or ψ_i^y at time t_i . An analogous computation to Eq. (E5) similarly reveals the apparent chaoticity of the Lindblad-Bernoulli shift according to ζ if the correction unitary is chosen to trivially be the identity matrix. However, if we allow V to be a unit-depth circuit, from Eq. (22) we arrive at

$$\begin{aligned} \zeta(\Upsilon^{(\text{LB})}) &= \sup_{V \in \mathcal{R}_{\text{MPO}}} \left(|\langle \Upsilon_{R|\vec{x}}^{(\text{LB})} | V | \Upsilon_{R|\vec{y}}^{(\text{LB})} \rangle|^2 \right) \\ &= \sup_{V \in \mathcal{R}_{\text{MPO}}} \left(|\langle \psi'_{SE|\vec{x}} | V | \psi'_{SE|\vec{y}} \rangle|^2 \right) \\ &= \sup_{V \in \mathcal{R}_{\text{MPO}}} |\langle \psi_1^x \cdots \psi_k^x \phi_{k+1} \cdots \phi_n | \\ &\quad V | \psi_1^y \cdots \psi_k^y \phi_{k+1} \cdots \phi_n \rangle|^2 = 1, \end{aligned} \quad (\text{E6})$$

where in the final line V is chosen in the supremum to align the k orthogonal sites of the final state with local unitaries, rendering $|\psi_i^x\rangle = |\psi_i^y\rangle$. This value being equal to one is indicative of the regularity of the dynamical system according to (C3). This example illustrates the advantage of the complete quantum chaos diagnostic defined in Eq. (22). If the effect of the butterfly flutter spreads in a complex way in the final state, then no simple V will be able to completely align the final states. This is what the scrambling criterion (C2) distinguishes.

Much like the Peres-Loschmidt echo, dynamical entropy cannot tell that the Lindblad-Bernoulli shift is regular. From the Choi representation given in Eq. (E4), we arrive immediately at a nonzero value,

$$S_{\text{Dy}}^{(k)}(\Upsilon^{(\text{LB})}) = \frac{kS(V\phi_i \otimes \frac{\mathbb{1}}{d_S})}{k} = \log(d_S). \quad (\text{E7})$$

In fact, Lindblad originally introduced this as a simple example of a chaotic process, given that it is unpredictable under repeated measurements [3]. The stronger conditions (C2)–(C3) show directly that he was mistaken and that this dynamics is highly regular.

We note that in Ref. [108] an example similar to the Lindblad-Bernoulli shift can be found, with dynamics generated by Chebotarev-Gregoratti Hamiltonians. These models would exhibit similar properties of apparent chaoticity according to the Peres-Loschmidt echo but for an infinite environment and valid for continuous time evolution. We have examined the simpler Lindblad-Bernoulli shift here as it is comparably instructive, and also to remain within the paradigm of finite-dimensional isolated quantum systems.

APPENDIX F: TYPICAL QUANTUM PROCESSES AND THEIR ENTANGLEMENT STRUCTURE

Here, we explain and utilize the main results from Refs. [59,60], to prove concentration-of-measure bounds for typical processes. These results state that processes generated from random evolution—be it fully Haar random or from an ϵ -approximate t -design—are likely to look Markovian when one only has access to repeated measurements on a small subsystem compared to the full unitarily evolving isolated system. In order to prove this result, Refs. [59,60] argue that in processes generated from random evolution, the Choi state is typically close to being maximally mixed and therefore has little memory. For us, this means directly that the purified process (as described in Sec. II) must be volume-law entangled. The following result will therefore follow rather directly from the proofs of Refs. [59,60].

Theorem 3.—(Most Processes Are Chaotic) Consider a pure process $|\Upsilon\rangle$ generated by random dynamics, either entirely Haar random, denoted by \mathbb{H} , or according to an ϵ -approximate t -design, denoted by $\mu_{\epsilon-t}$. Then, for any $R_1 \subset R$ such that $d_{R_1} \approx d_S$, and for any $\delta > 0$ and $0 < m < t/4$,

$$\mathbb{P}_{U_i \sim \mu} \left\{ \log(d_{BR_1}) - S^{(2)}(\Upsilon_{BR_1}) \geq \mathcal{J}_\mu(\delta) \right\} \leq \mathcal{G}_\mu(\delta). \quad (48)$$

where for a process generated from independent Haar-random evolution,

$$\begin{aligned} \mathcal{J}_{\mathbb{H}}(\delta) &= \log(d_{BR_1}(\mathcal{B} + \delta) + 1) \approx d_{BR_1} \left(\frac{1}{d_R} + \delta \right), \text{ and} \\ \mathcal{G}_{\mathbb{H}}(\delta) &= \exp[-\mathcal{C}\delta^2] \approx \exp\left[-\frac{(k+1)d_R}{8d_B}\delta^2\right], \end{aligned} \quad (49)$$

while for that generated from an ϵ -approximate unitary t -design,

$$\begin{aligned} \mathcal{J}_{\mu_{\epsilon-t}}(\delta) &= \log(d_{BR_1}\delta + 1) \approx d_{BR_1}\delta, \text{ and} \\ \mathcal{G}_{\mu_{\epsilon-t}}(\delta) &= \frac{\mathcal{F}(d_B, d_R, m, t, \epsilon)}{\delta^m}. \end{aligned} \quad (50)$$

The exact definitions of \mathcal{B} , \mathcal{C} , and \mathcal{F} are provided in Eqs. (F3), (F8) and (F10), respectively. The approximations in Eqs. (49) and (50) are valid for $d_R \gg d_B \gg 1$ and for small δ .

Proof.—We will utilize Levy’s lemma, which states that for some probability measure σ , and function $f(x)$ with $\delta > 0$,

$$\mathbb{P}_{x \sim \sigma} \{f(x) \geq \mathbb{E}_\sigma(f) + \delta\} \leq \alpha_\sigma(\delta/L), \quad (F1)$$

where $L > 0$ is the Lipschitz constant of f , which dictates how slowly varying f is in the measure space σ . The function α_σ is the concentration rate, which we require to be

vanishing in increasing δ to describe a concentration of measure [8].

For our purposes, σ will either be the full Haar measure \mathbb{H} or an ϵ -approximate t -design $\mu_{\epsilon-t}$ and $f(x)$ will be the deviation from maximum spatiotemporal entanglement, $\log(d_{BR_1}) - S^{(2)}(\Upsilon_{BR_1})$.

We first review and modify the results of Refs. [59,60], from which we define a concentration-of-measure result for $U_i \sim \mathbb{H}$ and $U_i \sim \mu_{\epsilon-t}$, respectively.

In both cases, we will arrive at the general form of the concentration of measure,

$$\mathbb{P}_{U_i \sim \mu} \left\{ \left\| \Upsilon_{BR_1} - \frac{\mathbb{1}}{d_{BR_1}} \right\|_2^2 \geq \mathcal{J}'_\mu(\delta) \right\} \leq \mathcal{G}_\mu(\delta). \quad (F2)$$

Theorem 3 will then follow from Eq. (F2), which we show at the end. \blacksquare

1. Process from Haar-random evolution

For dynamics generated by independent Haar-random unitaries, given that $d_{BR_1} = d_S^{2k} d_{R_1} \approx d_S^{2k+1} < d_E \approx d_R$, the Haar average of the left-hand side of the inequality within the brackets of Eq. (F3) is

$$\begin{aligned} \mathbb{E}_{\mathbb{H}} \left(\left\| \Upsilon_{BR_1} - \frac{\mathbb{1}_{BR_1}}{d_{BR_1}} \right\|_2^2 \right) &= \mathbb{E}_{\mathbb{H}}(\text{tr}(\Upsilon_{BR_1}^2)) - \frac{1}{d_{BR_1}} \\ &= \frac{d_E^2 - 1}{d_E(d_{SE} + 1)} \left(\frac{d_E^2 - 1}{d_{SE}^2 - 1} \right)^k + \frac{1}{d_E} - \frac{1}{d_S^{2k+1}} \\ &=: \mathcal{B}. \end{aligned} \quad (F3)$$

This is proved in Ref. [59, Appendix F]. Our setup is, however, a slightly modified version of this, as our final intervention is size d_{R_1} rather than d_S . In detail, as \mathcal{H}_{R_1} is the final intervention space, one can modify the result in Eq. (F3) by changing the factors \mathcal{A} and \mathcal{B} in Eq. (74) in Ref. [59] to

$$\begin{aligned} \mathcal{A} &\rightarrow d_{SE} d_{R_2} (d_{R_2}^2 + d_{R_1}^2 - 2) \text{ and} \\ \mathcal{B} &\rightarrow d_{SE} d_{R_2} (d_{SE}^2 - 1), \end{aligned} \quad (F4)$$

where we recall that \mathcal{H}_{R_2} is the complement to \mathcal{H}_{R_1} , such that $\mathcal{H}_{R_1} \otimes \mathcal{H}_{R_2} = \mathcal{H}_R$. Using this to simplify [59, Eq. (74)], we arrive at a long messy expression. However, it has same asymptotic behavior as Eq. (F3). More precisely, we make the approximation that $d_{R_1} \approx d_S \ll d_E$ —which is valid for the assumption that $d_{R_1} \ll d_R$.

In particular, if $d_E \gg 1$, such that $d_E - 1 \approx d_E$, then in both cases,

$$\mathbb{E}_{\mathbb{H}} \left(\left\| \Upsilon_{BR_1} - \frac{\mathbb{1}_{BR_1}}{d_{BR_1}} \right\|_2^2 \right) \approx \frac{1}{d_E}. \quad (F5)$$

Now, the concentration rate is the exponential function

$$\exp\left(\frac{-\delta^2(k+1)d}{4L^2}\right), \quad (\text{F6})$$

which is proved in Ref. [59, Appendixes]. Now, the Lipschitz constants can also be bounded by almost the same quantity as in Ref. [59], despite here having $f := \|\rho - \mathbb{1}/d\|_2^2$ compared to $(1/2)\|\rho - \mathbb{1}/d\|_1$. This is because we can use that $\|X\|_2^2 \leq \|X\|_2 \leq \|X\|_1$, where we also have an additional factor of 2 in L , given the factor of 1/2 in the definition of non-Markovianity, \mathcal{N} , in [59]. We therefore arrive at

$$\mathbb{P}\left\{\|\Upsilon_{BR_1} - \frac{\mathbb{1}}{d_{BR_1}}\|_2^2 > \mathcal{B} + \delta\right\} \leq \exp[-\mathcal{C}\delta^2] \quad (\text{F7})$$

for \mathcal{B} defined in Eq. (F3) and

$$\begin{aligned} \mathcal{C} &:= \frac{(k+1)d_E d_S (d_S - 1)^2}{8(d_S^{k+1} - 1)^2} \\ &= \frac{(k+1)d_E d_S}{8(d_S^k + d_S^{k-1} + \dots + 1)^2} \end{aligned} \quad (\text{F8})$$

defined from the above considerations. Again, we have taken the approximation that $d_{R_1} \approx d_S$.

2. Process from approximate unitary t -designs

If evolution is instead sampled from an ϵ -approximate t -design, we can adapt the results from Ref. [60], which in turn build on the deviation bounds for k -design results of Ref. [109]. The concentration-of-measure bound takes the form

$$\begin{aligned} \mathcal{F} &:= \left\{ \left[\frac{16m}{(k+1)d_{SE}} \left(\frac{d_S^{k+1} - 1}{d_S - 1} \right)^2 \right]^m + (\mathcal{B})^m \right. \\ &\quad \left. + \frac{\epsilon}{16^m d_{SE}^m} \left(d_E^k d_S^{2(k+2)} + \frac{1}{d_S^{2(k+1)}} \right) \right\}, \end{aligned} \quad (\text{F9})$$

for any $0 < m \leq t/4$, and $\delta > 0$. m can be chosen to optimize this bound and, overall, \mathcal{F} is small for $d_E \gg d_S^{2k+1} = d_{BR_1}$, for a high t . See Ref. [60] for further details and a proof for the above expression Eq. (F9). Here, we have slightly modified that result, as our object of interest is $\|\Upsilon_{BR_1} - \mathbb{1}/d_{BR_1}\|_2^2$ rather than a non-Markovianity measure. This means that we replace $\mathcal{N}_\bullet \rightarrow \|\Upsilon_{BR_1} - \mathbb{1}/d_{BR_1}\|_2^2$ and $\delta \rightarrow \sqrt{\delta}/2$ and we do not have the $d_S^{3(2k+1)}$ factor on the right-hand side of Ref. [60, Theorem 1]. In addition, we have made the same approximation as that considered above in Sec. F 1, in that we take $d_{R_1} \approx d_S$, which is valid for the asymptotic case where $d_E \gg d_{R_1}$.

Now, to complete the proof, we note that

$$\begin{aligned} \|\Upsilon_{BR_1} - \frac{\mathbb{1}}{d_{BR_1}}\|_2^2 &\geq \mathcal{J}'_\mu(\delta) \\ \iff \text{tr}(\Upsilon_{BR_1}^2) - \frac{1}{d_{BR_1}} &\geq \mathcal{J}'_\mu(\delta) \\ \iff S^{(2)}(\Upsilon_{BR_1}) &\leq -\log\left(\frac{d_{BR_1} \mathcal{J}'_\mu(\delta)}{d_{BR_1}} + \frac{1}{d_{BR_1}}\right) \\ \iff \log(d_{BR_1}) - S^{(2)}(\Upsilon_{BR_1}) &\geq \log(d_{BR_1} \mathcal{J}'_\mu(\delta) + 1), \end{aligned} \quad (\text{F10})$$

where $S^{(2)}$ is the 2-Rényi entropy. Substituting this into the probability brackets of Eq. (48), we arrive at Eq. (F1), with

$$\mathcal{J}_\mu(\delta) := \log(d_{BR_1} \mathcal{J}'_\mu(\delta) + 1). \quad (\text{F11})$$

-
- [1] J. Kudler-Flam, L. Nie, and S. Ryu, Conformal field theory and the web of quantum chaos diagnostics, *J. High Energy Phys.* **2020**, 175 (2020).
 - [2] M. V. Berry, M. Tabor, and J. M. Ziman, Level clustering in the regular spectrum, *Proc. R. Soc. London. A. Mathematical and Physical Sciences* **356**, 375 (1977).
 - [3] G. Lindblad, in *Fundamental Aspects of Quantum Theory*, edited by V. Gorini and A. Frigerio (Plenum Press, New York, 1986), p. 199.
 - [4] L. Reichl, *The Transition to Chaos: Conservative Classical and Quantum Systems* (Springer Nature, Cham, Switzerland, 2021), Vol. 200.
 - [5] F. Haake, S. Gnutzmann, and M. Kuś, *Quantum Signatures of Chaos* (Springer Science & Business Media, Cham, 2018).
 - [6] P. Hayden and J. Preskill, Black holes as mirrors: Quantum information in random subsystems, *J. High Energy Phys.* **2007**, 120 (2007).
 - [7] S. H. Shenker and D. Stanford, Black holes and the butterfly effect, *J. High Energy Phys.* **2014**, 67 (2014).
 - [8] S. Popescu, A. J. Short, and A. Winter, Entanglement and the foundations of statistical mechanics, *Nat. Phys.* **2**, 754 (2006).
 - [9] C. Gogolin and J. Eisert, Equilibration, thermalisation, and the emergence of statistical mechanics in closed quantum systems, *Rep. Prog. Phys.* **79**, 056001 (2016).
 - [10] L. D'Alessio, Y. Kafri, A. Polkovnikov, and M. Rigol, From quantum chaos and eigenstate thermalization to statistical mechanics and thermodynamics, *Adv. Phys.* **65**, 239 (2016).
 - [11] A. Peres, Stability of quantum motion in chaotic and regular systems, *Phys. Rev. A* **30**, 1610 (1984).
 - [12] J. Emerson, Y. S. Weinstein, S. Lloyd, and D. G. Cory, Fidelity decay as an efficient indicator of quantum chaos, *Phys. Rev. Lett.* **89**, 284102 (2002).
 - [13] P. Pechukas, Kolmogorov entropy and ‘‘quantum chaos’’, *J. Phys. Chem.* **86**, 2239 (1982).

- [14] W. Ślomeczyński and K. Życzkowski, Quantum chaos: An entropy approach, *J. Math. Phys.* **35**, 5674 (1994).
- [15] R. Alicki and M. Fannes, Defining quantum dynamical entropy, *Lett. Math. Phys.* **32**, 75 (1994).
- [16] T. c. v. Prosen and M. Žnidarič, Is the efficiency of classical simulations of quantum dynamics related to integrability?, *Phys. Rev. E* **75**, 015202(R) (2007).
- [17] T. c. v. Prosen and I. Pižorn, Operator space entanglement entropy in a transverse Ising chain, *Phys. Rev. A* **76**, 032316 (2007).
- [18] B. Bertini, P. Kos, and T. Prosen, Operator entanglement in local quantum circuits I: Chaotic dual-unitary circuits, *SciPost Phys.* **8**, 067 (2020).
- [19] P. Hosur, X.-L. Qi, D. A. Roberts, and B. Yoshida, Chaos in quantum channels, *J. High Energy Phys.* **2016**, 4 (2016).
- [20] These are a selection of some of the most popularly accepted chaos probes but this is by no means an exhaustive list. For example, some interesting alternative measures are entanglement spectrum statistics [91], the spectral form factor [5], and quantum coherence measures [110]. Also see Refs. [1,111] and references therein.
- [21] J. M. Deutsch, Quantum statistical mechanics in a closed system, *Phys. Rev. A* **43**, 2046 (1991).
- [22] M. Srednicki, Chaos and quantum thermalization, *Phys. Rev. E* **50**, 888 (1994).
- [23] M. Rigol, V. Dunjko, and M. Olshanii, Thermalization and its mechanism for generic isolated quantum systems, *Nature* **452**, 854 EP (2008).
- [24] B. Yan, L. Cincio, and W. H. Zurek, Information scrambling and Loschmidt echo, *Phys. Rev. Lett.* **124**, 160603 (2020).
- [25] D. A. Roberts and B. Yoshida, Chaos and complexity by design, *J. High Energy Phys.* **2017**, 121 (2017).
- [26] L. Leone, S. F. E. Oliviero, and A. Hamma, Isospectral twirling and quantum chaos, *Entropy* **23**, 1073 (2021).
- [27] D. A. Roberts, D. Stanford, and L. Susskind, Localized shocks, *J. High Energy Phys.* **2015**, 51 (2015).
- [28] S. Pilatowsky-Cameo, J. Chávez-Carlos, M. A. Bastarrachea-Magnani, P. Stránský, S. Lerma-Hernández, L. F. Santos, and J. G. Hirsch, Positive quantum Lyapunov exponents in experimental systems with a regular classical limit, *Phys. Rev. E* **101**, 010202(R) (2020).
- [29] T. Xu, T. Scaffidi, and X. Cao, Does scrambling equal chaos?, *Phys. Rev. Lett.* **124**, 140602 (2020).
- [30] N. Dowling, P. Kos, and K. Modi, Scrambling is necessary but not sufficient for chaos, *Phys. Rev. Lett.* **131**, 180403 (2023).
- [31] F. A. Pollock, C. Rodríguez-Rosario, T. Frauenheim, M. Paternostro, and K. Modi, Non-Markovian quantum processes: Complete framework and efficient characterization, *Phys. Rev. A* **97**, 012127 (2018).
- [32] F. A. Pollock, C. Rodríguez-Rosario, T. Frauenheim, M. Paternostro, and K. Modi, Operational Markov condition for quantum processes, *Phys. Rev. Lett.* **120**, 040405 (2018).
- [33] S. Milz and K. Modi, Quantum stochastic processes and quantum non-Markovian phenomena, *PRX Quantum* **2**, 030201 (2021).
- [34] S. Milz, F. A. Pollock, and K. Modi, An introduction to operational quantum dynamics, *Open Syst. Inf. Dyn.* **24**, 1740016 (2017).
- [35] G. Chiribella, G. M. D’Ariano, and P. Perinotti, Quantum circuit architecture, *Phys. Rev. Lett.* **101**, 060401 (2008).
- [36] J. Watrous, *The Theory of Quantum Information* (Cambridge University Press, Cambridge, UK, 2018).
- [37] F. Costa and S. Shrapnel, Quantum causal modelling, *New J. Phys.* **18**, 063032 (2016).
- [38] P. Taranto, F. A. Pollock, S. Milz, M. Tomamichel, and K. Modi, Quantum Markov order, *Phys. Rev. Lett.* **122**, 140401 (2019).
- [39] P. Taranto, S. Milz, F. A. Pollock, and K. Modi, Structure of quantum stochastic processes with finite Markov order, *Phys. Rev. A* **99**, 042108 (2019).
- [40] N. Dowling, P. Figueroa-Romero, F. A. Pollock, P. Strasberg, and K. Modi, Relaxation of multitime statistics in quantum systems, *Quantum* **7**, 1027 (2023).
- [41] N. Dowling, P. Figueroa-Romero, F. A. Pollock, P. Strasberg, and K. Modi, Equilibration of multitime quantum processes in finite time intervals, *SciPost Phys. Core* **6**, 043 (2023).
- [42] P. Strasberg and M. G. Díaz, Classical quantum stochastic processes, *Phys. Rev. A* **100**, 022120 (2019).
- [43] S. Milz, D. Egloff, P. Taranto, T. Theurer, M. B. Plenio, A. Smirne, and S. F. Huelga, When is a non-Markovian quantum process classical?, *Phys. Rev. X* **10**, 041049 (2020).
- [44] P. Strasberg, A. Winter, J. Gemmer, and J. Wang, Classcality, Markovianity and local detailed balance from pure state dynamics (2022).
- [45] S. Milz, C. Spee, Z.-P. Xu, F. A. Pollock, K. Modi, and O. Gühne, Genuine multipartite entanglement in time, *SciPost Phys.* **10**, 141 (2021).
- [46] G. A. L. White, F. A. Pollock, L. C. L. Hollenberg, C. D. Hill, and K. Modi, From many-body to many-time physics, [arXiv:2107.13934](https://arxiv.org/abs/2107.13934) [quant-ph] (2021).
- [47] J. Eisert, M. Cramer, and M. B. Plenio, Colloquium: Area laws for the entanglement entropy, *Rev. Mod. Phys.* **82**, 277 (2010).
- [48] M. Fannes, B. Nachtergaele, and R. F. Werner, Finitely correlated states on quantum spin chains, *Commun. Math. Phys.* **144**, 443 (1992).
- [49] N. Schuch, M. M. Wolf, F. Verstraete, and J. I. Cirac, Entropy scaling and simulability by matrix product states, *Phys. Rev. Lett.* **100**, 030504 (2008).
- [50] J. C. Bridgeman and C. T. Chubb, Hand-waving and interpretive dance: An introductory course on tensor networks, *J. Phys. A: Math. Theor.* **50**, 223001 (2017).
- [51] G. Vidal, J. I. Latorre, E. Rico, and A. Kitaev, Entanglement in quantum critical phenomena, *Phys. Rev. Lett.* **90**, 227902 (2003).
- [52] This is in reference to its introduction in Ref. [3] and the chaotic classical analogy of the Bernoulli shift.
- [53] J. Cotler, C.-M. Jian, X.-L. Qi, and F. Wilczek, Superdensity operators for spacetime quantum mechanics, *J. High Energy Phys.* **2018**, 93 (2018).
- [54] E. H. Lieb and D. W. Robinson, The finite group velocity of quantum spin systems, *Commun. Math. Phys.* **28**, 251 (1972).
- [55] C.-F. Chen, A. Lucas, and C. Yin, Speed limits and locality in many-body quantum dynamics, *Rep. Prog. Phys.* **86**, 116001 (2023).

- [56] C. W. von Keyserlingk, T. Rakovszky, F. Pollmann, and S. L. Sondhi, Operator hydrodynamics, OTOCs, and entanglement growth in systems without conservation laws, *Phys. Rev. X* **8**, 021013 (2018).
- [57] A. Nahum, J. Ruhman, S. Vijay, and J. Haah, Quantum entanglement growth under random unitary dynamics, *Phys. Rev. X* **7**, 031016 (2017).
- [58] D. A. Roberts and B. Swingle, Lieb-Robinson bound and the butterfly effect in quantum field theories, *Phys. Rev. Lett.* **117**, 091602 (2016).
- [59] P. Figueroa-Romero, K. Modi, and F. A. Pollock, Almost Markovian processes from closed dynamics, *Quantum* **3**, 136 (2019).
- [60] P. Figueroa-Romero, F. A. Pollock, and K. Modi, Markovianization with approximate unitary designs, *Commun. Phys.* **4**, 127 (2021).
- [61] M. A. Nielsen, M. R. Dowling, M. Gu, and A. C. Doherty, Quantum computation as geometry, *Science* **311**, 1133 (2006).
- [62] L. Susskind, Computational complexity and black hole horizons, [arXiv:1402.5674](https://arxiv.org/abs/1402.5674) [quant-ph] (2014).
- [63] A. Bouland, B. Fefferman, and U. Vazirani, Computational pseudorandomness, the wormhole growth paradox, and constraints on the ADS/CFT duality, [arXiv:1910.14646](https://arxiv.org/abs/1910.14646) [quant-ph] (2019).
- [64] Y. Sekino and L. Susskind, Fast scramblers, *J. High Energy Phys.* **2008**, 065 (2008).
- [65] S. H. Shenker and D. Stanford, Multiple shocks, *J. High Energy Phys.* **2014**, 46 (2014).
- [66] This quantity is alternatively called fidelity decay or Loschmidt echo in the literature. We take the middle ground here, to give credit to the historical role of Peres [11], while remaining familiar to those who recognize this quantity as the latter.
- [67] D. Poulin, R. Blume-Kohout, R. Laflamme, and H. Ollivier, Exponential speedup with a single bit of quantum information: Measuring the average fidelity decay, *Phys. Rev. Lett.* **92**, 177906 (2004).
- [68] A. M. Childs, Y. Su, M. C. Tran, N. Wiebe, and S. Zhu, Theory of Trotter error with commutator scaling, *Phys. Rev. X* **11**, 011020 (2021).
- [69] G. Lindblad, Non-Markovian quantum stochastic processes and their entropy, *Commun. Math. Phys.* **65**, 281 (1979).
- [70] S. Milz, F. Sakuldee, F. A. Pollock, and K. Modi, Kolmogorov extension theorem for (quantum) causal modelling and general probabilistic theories, *Quantum* **4**, 255 (2020).
- [71] R. A. Jalabert and H. M. Pastawski, Environment-independent decoherence rate in classically chaotic systems, *Phys. Rev. Lett.* **86**, 2490 (2001).
- [72] F. M. Cucchietti, C. H. Lewenkopf, E. R. Mucciolo, H. M. Pastawski, and R. O. Vallejos, Measuring the Lyapunov exponent using quantum mechanics, *Phys. Rev. E* **65**, 046209 (2002).
- [73] J. Maldacena, S. H. Shenker, and D. Stanford, A bound on chaos, *J. High Energy Phys.* **2016**, 106 (2016).
- [74] L. Foini and J. Kurchan, Eigenstate thermalization hypothesis and out of time order correlators, *Phys. Rev. E* **99**, 042139 (2019).
- [75] D. E. Parker, X. Cao, A. Avdoshkin, T. Scaffidi, and E. Altman, A universal operator growth hypothesis, *Phys. Rev. X* **9**, 041017 (2019).
- [76] The classical Pesin's theorem states that the Kolmogorov-Sinai entropy is a lower bound of the sum of the positive Lyapunov exponents of a classical dynamical system [112].
- [77] I. Pižorn and T. c. v. Prosen, Operator space entanglement entropy in XY spin chains, *Phys. Rev. B* **79**, 184416 (2009).
- [78] D. Muth, R. G. Unanyan, and M. Fleischhauer, Dynamical simulation of integrable and nonintegrable models in the Heisenberg picture, *Phys. Rev. Lett.* **106**, 077202 (2011).
- [79] J. Dubail, Entanglement scaling of operators: A conformal field theory approach, with a glimpse of simulability of long-time dynamics in 1+1d, *J. Phys. A: Math. Theor.* **50**, 234001 (2017).
- [80] C. Jonay, D. A. Huse, and A. Nahum, Coarse-grained dynamics of operator and state entanglement, [arXiv:1803.00089](https://arxiv.org/abs/1803.00089) [cond-mat.stat-mech] (2018).
- [81] V. Alba, J. Dubail, and M. Medenjak, Operator entanglement in interacting integrable quantum systems: The case of the Rule 54 chain, *Phys. Rev. Lett.* **122**, 250603 (2019).
- [82] V. Alba, Diffusion and operator entanglement spreading, *Phys. Rev. B* **104**, 094410 (2021).
- [83] M. Heyl, P. Hauke, and P. Zoller, Quantum localization bounds Trotter errors in digital quantum simulation, *Sci. Adv.* **5**, eaau8342 (2019).
- [84] M. Santhanam, S. Paul, and J. B. Kannan, Quantum kicked rotor and its variants: Chaos, localization and beyond, *Phys. Rep.* **956**, 1 (2022), [quantum kicked rotor and its variants: Chaos, localization and beyond](https://arxiv.org/abs/2205.12345).
- [85] F. Alet and N. Laflorencie, Many-body localization: An introduction and selected topics, *C. R. Phys.* **19**, 498 (2018).
- [86] S. D. Geraedts, R. Nandkishore, and N. Regnault, Many-body localization and thermalization: Insights from the entanglement spectrum, *Phys. Rev. B: Condens. Matter* **93**, 174202 (2016).
- [87] B. Skinner, J. Ruhman, and A. Nahum, Measurement-induced phase transitions in the dynamics of entanglement, *Phys. Rev. X* **9**, 031009 (2019).
- [88] L. Zhang, J. A. Reyes, S. Kourtis, C. Chamon, E. R. Mucciolo, and A. E. Ruckenstein, Nonuniversal entanglement level statistics in projection-driven quantum circuits, *Phys. Rev. B* **101**, 235104 (2020).
- [89] D. Poulin, A. Qarry, R. Somma, and F. Verstraete, Quantum simulation of time-dependent Hamiltonians and the convenient illusion of Hilbert space, *Phys. Rev. Lett.* **106**, 170501 (2011).
- [90] Y. Nakata, C. Hirche, M. Koashi, and A. Winter, Efficient quantum pseudorandomness with nearly time-independent Hamiltonian dynamics, *Phys. Rev. X* **7**, 021006 (2017).
- [91] C. Chamon, A. Hamma, and E. R. Mucciolo, Emergent irreversibility and entanglement spectrum statistics, *Phys. Rev. Lett.* **112**, 240501 (2014).
- [92] E. Bianchi, L. Hackl, M. Kieburg, M. Rigol, and L. Vidmar, Volume-law entanglement entropy of typical pure quantum states, *PRX Quantum* **3**, 030201 (2022).

- [93] M. Serbyn, D. A. Abanin, and Z. Papić, Quantum many-body scars and weak breaking of ergodicity, *Nat. Phys.* **17**, 675 (2021).
- [94] S. Moudgalya, B. A. Bernevig, and N. Regnault, Quantum many-body scars and Hilbert space fragmentation: a review of exact results, *Rep. Prog. Phys.* **85**, 086501 (2022).
- [95] M. J. Bremner, C. Mora, and A. Winter, Are random pure states useful for quantum computation?, *Phys. Rev. Lett.* **102**, 190502 (2009).
- [96] D. Gross, S. T. Flammia, and J. Eisert, Most quantum states are too entangled to be useful as computational resources, *Phys. Rev. Lett.* **102**, 190501 (2009).
- [97] J. P. Crutchfield, Between order and chaos, *Nat. Phys.* **8**, 17 (2012).
- [98] G. Vidal, Entanglement renormalization, *Phys. Rev. Lett.* **99**, 220405 (2007).
- [99] N. Dowling, K. Modi, R. N. Muñoz, S. Singh, and G. A. L. White, Process tree: Efficient representation of quantum processes with complex long-range memory, [arXiv:2312.04624](https://arxiv.org/abs/2312.04624) [quant-ph] (2023).
- [100] W. H. Zurek, Decoherence, einselection, and the quantum origins of the classical, *Rev. Mod. Phys.* **75**, 715 (2003).
- [101] L. Leone, S. F. E. Oliviero, Y. Zhou, and A. Hamma, Quantum chaos is quantum, *Quantum* **5**, 453 (2021).
- [102] G. Chiribella, G. M. D’Ariano, and P. Perinotti, Theoretical framework for quantum networks, *Phys. Rev. A* **80**, 022339 (2009).
- [103] O. Oreshkov and C. Giarmatzi, Causal and causally separable processes, *New J. Phys.* **18**, 093020 (2016).
- [104] S. Shrapnel, F. Costa, and G. Milburn, Updating the Born rule, *New J. Phys.* **20**, 053010 (2018).
- [105] Markov’s inequality states that for any non-negative random variable X with mean $\mathbb{E}(X)$ and for any $\delta > 0$, $\mathbb{P}\{X \geq \delta\} \leq \mathbb{E}(X)/\delta$.
- [106] By this, we mean that the process $|\Upsilon\rangle$ has a freedom in choosing what the “actual” initial state is. One has a gauge freedom in choosing any initial state that would tomographically lead to the same state $|\Upsilon\rangle$.
- [107] Generalized Pauli operators on a d -dimensional space are defined by the generators [25]
- $$X|n\rangle = |n+1\rangle, \quad \text{and} \quad Z|n\rangle = \exp[2\pi in/d]|n\rangle. \quad (51)$$
- [108] D. Burgarth, P. Facchi, M. Ligabò, and D. Lonigro, Hidden non-Markovianity in open quantum systems, *Phys. Rev. A* **103**, 012203 (2021).
- [109] R. A. Low, Large deviation bounds for k -designs, *Proc. R. Soc. A: Mathematical, Phys. Eng. Sci.* **465**, 3289 (2009).
- [110] N. Anand, G. Styliaris, M. Kumari, and P. Zanardi, Quantum coherence as a signature of chaos, *Phys. Rev. Res.* **3**, 023214 (2021).
- [111] N. Hunter-Jones, Ph.D. thesis, Institute for Quantum Information and Matter, California Institute of Technology, 2018.
- [112] Y. Pesin, Characteristic Lyapunov exponents and smooth ergodic theory, *Russian Mathematical Surveys* **32**, 55 (1977).